Structural Engineering and Mechanics, *Vol. 72, No. 1 (2019) 113-129*
DOI: https://doi.org/10.12989/sem.2019.72.1.113

Assessment of porosity influence on dynamic characteristics of smart heterogeneous magneto-electro-elastic plates

Farzad Ebrahimi*[1], Ali Jafari[1] and Vinyas Mahesh[2]

[1]*Department of Mechanical Engineering, Faculty of Engineering, Imam Khomeini International University, Qazvin, Iran*
[2]*Department of Mechanical Engineering, Nitte Meenakshi Institute of Technology, Bangalore, India*

(Received May 25, 2018, Revised April 19, 2019, Accepted May 14, 2019)

Abstract. A four-variable shear deformation refined plate theory has been proposed for dynamic characteristics of smart plates made of porous magneto-electro-elastic functionally graded (MEE-FG) materials with various boundary conditions by using an analytical method. Magneto-electro-elastic properties of FGM plate are supposed to vary through the thickness direction and are estimated through the modified power-law rule in which the porosities with even and uneven type are approximated. Pores possibly occur inside functionally graded materials (FGMs) due the result of technical problems that lead to creation of micro-voids in these materials. The variation of pores along the thickness direction influences the mechanical properties. The governing differential equations and boundary conditions of embedded porous FGM plate under magneto-electrical field are derived through Hamilton's principle based on a four-variable tangential-exponential refined theory which avoids the use of shear correction factors. An analytical solution procedure is used to achieve the natural frequencies of embedded porous FG plate supposed to magneto-electrical field with various boundary condition. A parametric study is led to carry out the effects of material graduation exponent, coefficient of porosity, magnetic potential, electric voltage, elastic foundation parameters, various boundary conditions and plate side-to-thickness ratio on natural frequencies of the porous MEE-FG plate. It is concluded that these parameters play significant roles on the dynamic behavior of porous MEE-FG plates. Presented numerical results can serve as benchmarks for future analyses of MEE-FG plates with porosity phases.

Keywords: Magneto-electro-elastic FG plate; Porous materials; Free vibration; Refined plate theory

1. Introduction

Magneto-electro-elastic materials (MEEMs) as one of the special sorts of smart materials have received much attention in engineering structures during the recent years. In 1990s, in two-phase composites of piezoelectric and piezo-magnetic materials, a strong magneto-electrical coupling effect was discovered which has potential practical application in many fields (Benveniste, 1995) and reported that this coupling effect cannot be found in a single phase material. Furthermore, MEE materials shows some fascinating properties such as the piezo-electric, piezo-magnetic and magneto-electric influences in which the elastic deformations may be produced directly by mechanical loading or indirectly by an application of electric or magnetic field. The mechanical behaviors of magneto-electro-elastic structures have received notable attention by many researchers in the recent years. Among them, analytical solutions for studying magneto-electro-elastic responses of beams is presented by Jiang and Ding (2004). Chen *et al*. (2005) investigated vibrational responses of non-homogeneous isotropic MEE plates. Vibration characteristics of multiphase and layered magneto-electro-elastic beam is reported by Annigeri *et al*. (2007). Kumaravel *et al*. (2007) researched thermal stability and vibrational behavior of layered and multiphase magneto-electro-elastic beams. By implementation of finite element method, transient dynamic response of multiphase magneto-electro-elastic cantilever beam is presented by Daga *et al*. (2009). Also, Liu and Chang (2010) provided closed solution for the vibration of an isotropic magneto-electro-elastic plate. Razavi and Shooshtari (2015) presented nonlinear vibration investigation of a magneto-electro-elastic laminated plate with all edges simply supported. They employed the first order shear deformation theory considering the von Karman's nonlinear strains to obtain the equations of motion, whereas Maxwell equations for electrostatics and magneto-statics are used to model the electric and magnetic behavior. Most recently, based on three-dimensional elasticity theory and employing the state space approach, Xin and Hu (2015) presented semi-analytical evaluation of free vibration of arbitrary layered magneto-electro-elastic beams.

Functionally graded materials (FGMs) as a new class of composite structures have drawn the attention of many researchers in the smart materials and structures by minimizing or removing stress concentrations at the interfaces of the traditional composite materials. The material properties of FGMs varies continuously in one or more directions. Recently, FGMs have received wide applications as structural components in modern industries such as mechanical, civil, nuclear reactors, and aerospace engineering.

*Corresponding author, Ph.D.
E-mail: febrahimy@eng.ikiu.ac.ir

ISSN: 1225-4568 (Print), 1598-6217 (Online)

In the recent years, several researchers examined mechanical properties of structural elements made from magneto-electro-elastic functionally graded (MEE-FG) materials. Pan and Han (2005) provided exact solution for analysis of the rectangular plates composed of functionally graded, anisotropic, and linear magneto-electro-elastic materials. Furthermore, the plane stress problem of a MEE-FG beam were inspected by Huang *et al*. (2007) using an analytical method. In another survey, Wu and Tsai (2007) examined static behavior of a doubly curved MEE-FG shell employing an asymptotic approach. Kattimani and Ray (2015) researched large amplitude vibration responses of MEE-FG plates. Static behavior of a circular MEE-FG plate is analyzed by Sladek *et al*. (2015) by using a meshless method. More recently, Vinyas and Kattimani contributed to the research community through their works which discuss the effect of various forms of thermal loading on the coupled static response of stepped-functionally graded MEE beams (Vinyas and Kattimani 2017a, b, c, d, e) and plates (Vinyas and Kattimani 2017f). Extending their evaluation on the same grounds, the influence of moisture was also briefed out (Vinyas and Kattimani 2017g; Vinyas *et al*. 2018). With the rapid progression in technology of structural elements, structures with graded porosity can be introduced as one of the latest development in FGMs. The structures consider pores into microstructures by taking the local density into account. Researches focus on development in preparation methods of FGMs such as powder metallurgy, vapor deposition, self-propagation, centrifugal casting, and magnetic separation (Peng *et al*. 2007). These methods have their own ineffectiveness such as high costs and complexity of the technique. An efficient way to manufacture FGMs is sintering process in which due to difference in solidification of the material constituents, porosities or micro-voids through material can create (Zhu *et al*. 2001). An investigation has been carried out on porosities existing in FGMs fabricated by a multi-step sequential infiltration technique (Wattanasakulpong *et al*.2012). According to this information about porosities in FGMs, it is necessary to study the porosity impact when designing and analyzing FGM structures. Porous FG structures have many interesting combinations of mechanical properties, such as high stiffness in conjunction with very law specific weight (Rezaei and Saidi 2016). A few studies on the vibration responses of porous FGM structures are available in literature. Wattanasakulpong and Ungbhakorn (2014) studied the linear and non-linear vibration of porous FGM beams with elastically restrained ends. Ebrahimi and Mokhtari (2014) utilized DT method to investigate vibration of rotating Timoshenko FG beams with even porosities. They reported that porosity volume fraction has a significant effect on the vibrational response of the FG beams. In order to predict flexural vibration of porous FGM Timoshenko beams, Wattanasakulpong and Chaikittiratana (2015) employed Chebyshev collocation method. Moreover, Ait Yahia *et al*. (2015) study the porosity effect on the wave propagation of FG plates by using various higher-order shear deformation theories. Ebrahimi and Zia (2015) applied the Galerkin and multiple scales methods to solve nonlinear vibration of porous FGM beams. Tang *et al*. (2018) investigated the buckling behaviour of two-directionally porous beam. Ebrahimi *et al*. (2016) presented thermo-mechanical vibration response of temperature-dependent porous FG beams subjected to various temperature risings. FG structures resting on elastic foundations have wide applications in modern engineering. The interaction of a plate with its foundation can be explained by suggesting various basic models in the literature (Shahsavari *et al*., 2018). One of the simplest model for the elastic foundation is Winkler model because it takes the foundation into account as a set of independent and separate springs. Pasternak improved this model later by introducing a new dependence parameter which takes the interactions between the separated springs in Winkler model into account. Many researchers use plates resting on foundations to model the interaction between elastic plates and media for many engineering problems. Ying *et al*. (2008) provided exact solution for bending and vibration embedded FG beam based on two dimensional elasticity theory. Thermo-mechanical vibration of FGM sandwich beam under variable elastic foundations by DQM analyzed by Pradhan and Murmu (2009). Temperature-dependent flexural wave propagation in nanoplate-type porous heterogenous material subjected to in-plane magnetic field was evaluated by Karami *et al*. (2018). 3-D free vibration of thick functionally graded plates on elastic foundations was examined by Malekzadeh (2009). Benchmark solutions for FG thick plates resting on Winkler–Pasternak elastic foundations was introduced by Huang *et al*. (2008).DSC method was utilized for non-linear analysis of laminated plates resting on Winkler–Pasternak elastic foundations firstly by Civalek and Akgoz (2011). Using DSC-HDQ coupled methodology and HDQ-FD coupled methodology, Civalek (2006, 2007) studied geometrically non-linear static and dynamic analysis of thin rectangular plates resting on Winkler–Pasternak elastic foundations. 3-D free vibration of thick circular plates on Pasternak foundation was introduced by Zhou *et al*. (2006). Also, 3-D free vibration analysis of annular plates on Pasternak elastic foundation by p-Ritz method was examined by Hosseini Hashemi *et al*. (2008). Atmane *et al*. (2015) applied an efficient beam theory to study the effects of thickness stretching and porosity on mechanical responses of FGM beams resting on elastic foundation. Recently, Mechab *et al*. (2016)developed a nonlocal elasticity model for free vibration of FG porous nanoplates resting on elastic foundations. Boutahar *et al*.(2016) presented a semi analytical method for non-linear vibration analysis of FGM porous annular plates resting on elastic foundations.

Literature search in the area of vibration analyses of FG porous plate indicates that there is not any published work considering magneto-electrical field and elastic foundation effects on vibration characteristics of FG plates with different porosity models based on four-variable refined shear deformation theory. This paper focuses on free vibration of magneto-electro-porous FG plates resting on elastic foundations with various boundary conditions based on a four-variable refined plate theory which provides a constant transverse displacement and higher-order variation of axial displacement through the depth of the plate so that

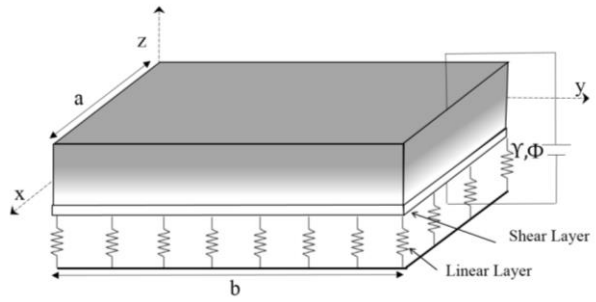

Fig. 1 Geometry of embedded FGM plate under magneto-electrical field

there is no need for any shear correction factors. Two kinds of porosity distribution namely even and uneven through the thickness directions are considered. The modified power-law model is exploited to describe gradual variation of material properties of the porous MEE-FG plate. Applying Hamilton's principle, governing equations of higher order MEE-FG plate are obtained together based on four-variable refined shear deformation theory and they are solved applying an analytical solution method. Several numerical exercises indicate that various parameters such as magnetic potential, external electric voltage, elastic foundation parameters, porosity volume fraction, types of porosity distribution, material graduation index and various boundary conditions have remarkable influence on fundamental frequencies of porous MEE-FG plate.

2. Theoretical formulations

2.1. The material properties of porous magneto-electro-elastic FG plates

Consider a magneto-electro-elastic functionally graded plate resting on elastic foundation with two different porosity distribution and rectangular cross-section of width *b* and thickness *h* according to Fig.1. Embedded MEE-FG plate is composed of $BaTio_3$ and $CoFe_2O_4$ materials with the material properties presented in Table 1 and exposed to a magnetic potential $\gamma(x,z,t)$ and electric potential $\Phi(x,z,t)$. The effective material properties of MEE-FG plate change continuously in the thickness direction according to modified power-law distribution. The effective material properties (P_f) of porous FGM plate by using the modified rule of mixture can be expressed by Wattanasakulpong and Ungbhakorn (2014)

$$P_f = P_u(V_u - \frac{\alpha}{2}) + P_l(V_l - \frac{\alpha}{2}) \tag{1}$$

In which α denotes the volume fraction of porosities, for a perfect FGM α is set to zero, P_u and P_l are the material properties of top and bottom sides, V_u and V_l are the volume fraction of top and bottom surfaces, respectively and are related by

$$V_u + V_l = 1 \tag{2}$$

Table 1 Magneto-electro-elastic coefficients of material properties

Properties	$BaTiO_3$	$CoFe_2O_4$
$c_{11} = c_{22}$ (GPa)	166	286
c_{33}	162	269.5
$c_{13} = c_{23}$	78	170.5
c_{12}	77	173
c_{55}	43	45.3
c_{66}	44.5	56.5
e_{31} (Cm^{-2})	-4.4	0
e_{33}	18.6	0
e_{15}	11.6	0
q_{31} (N/Am)	0	580.3
q_{33}	0	699.7
q_{15}	0	550
s_{11} ($10^{-9} C^2 m^{-2} N^{-1}$)	11.2	0.08
s_{33}	12.6	0.093
χ_{11}($10^{-6} Ns^2C^{-2}/2$)	5	-590
χ_{33}	10	157
$d_{11} = d_{22} = d_{33}$	0	0
ρ (kgm^{-3})	5800	5300

Then the volume fraction of upper side(V_u)is defined as follows

$$V_u = (\frac{z}{h} + \frac{1}{2})^P \tag{3}$$

where $(p \geq 0)$ is a non-negative parameter (power-law exponent or the volume fraction index) which determine the material distribution across the plate thickness.

According to Eqs. (1)- (2), the effective material properties of porous MEE-FG (I) plates with even porosities are variable across the thickness direction with the following form

$$P(z) = (P_u - P_l)\left(\frac{z}{h} + \frac{1}{2}\right)^P + P_l - (P_u + P_l)\frac{\alpha}{2} \tag{4}$$

It must be noted that, the top surface at $z=+h/2$ of embedded porous MEE-FG plate is fully $CoFe_2O_4$, whereas the bottom surface ($z=-h/2$) is fully $BaTio_3$. Moreover, the MEE-FG (II) plate has porosity phases spreading frequently nearby the middle zone of the cross-section and the amount of porosity seems to be linearly decrease to zero at the top and bottom of the cross-section. Fig. 2 demonstrates cross-section areas of FGM-I and-II with porosities phases. For uneven distribution of porosities, the effective material properties are replaced by following form.

$$P(z) = (P_u - P_l)\left(\frac{z}{h} + \frac{1}{2}\right)^P + P_l - \frac{\alpha}{2}(P_u + P_l)(1 - \frac{2|z|}{h}) \tag{5}$$

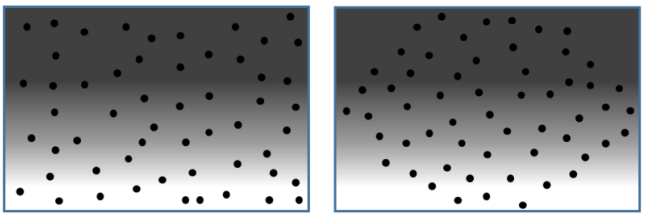

Fig. 2 Cross-section area of FGM plate with even and uneven porosities.

2.2 Kinematic relations

Based on new tangential-exponential refined shear deformation theory, the displacement field at any point of the plate can be expressed as

$$u_1(x,y,z,t)=u(x,y,t)-z\frac{\partial w_b}{\partial x}-f(z)\frac{\partial w_s}{\partial x} \quad (6)$$

$$u_2(x,y,z,t)=v(x,y,t)-z\frac{\partial w_b}{\partial y}-f(z)\frac{\partial w_s}{\partial y} \quad (7)$$

$$u_3(x,y,z,t)=w_b(x,y,t)+w_s(x,y,t) \quad (8)$$

In which u and v are displacement of mid-plane along x, y-axis and w_b, w_s are the bending and shear components of transverse displacement of a point on the mid-plane of the plate and t is the time. $f(z)$ denotes a shape function estimating the distribution of shear stress across the plate thickness. $f(z)$ is considered to satisfy the stress-free boundary conditions on the top and bottom sides of the plate. So it is not required to use any shear correction factor. The present theory has a function in the form (Mantari *et al*., 2014)

$$f(z)=\tan\left[\left(\frac{\pi(z)}{2h}\right)\right]r^{\sec\left[\left(\frac{\pi(z)}{2h}\right)\right]},\quad r=0.03 \quad (9)$$

The electric potential and magnetic potential distributions across the thickness are approximated via a combination of a cosine and linear variation to satisfy Maxwell's equation in the quasi-static approximation as follows (Ke *et al*. 2014)

$$\Phi(x,y,z,t)=-\cos(\xi(z+C))\phi(x,y,t)+\frac{2(z)}{h}V \quad (10)$$

$$\Upsilon(x,y,z,t)=-\cos(\xi(z))\gamma(x,y,t)+\frac{2(z)}{h}\Omega \quad (11)$$

where $\zeta = \pi/h$. Also, V and Ω are the external electric voltage and magnetic potential applied to the MEE-FG plate. Nonzero strains of the four-variable plate model are expressed by

$$\begin{Bmatrix}\varepsilon_x\\ \varepsilon_y\\ \gamma_{xy}\end{Bmatrix}=\begin{Bmatrix}\varepsilon_x^0\\ \varepsilon_y^0\\ \gamma_{xy}^0\end{Bmatrix}+z\begin{Bmatrix}\kappa_x^b\\ \kappa_y^b\\ \kappa_{xy}^b\end{Bmatrix}+f\begin{Bmatrix}\kappa_x^s\\ \kappa_y^s\\ \kappa_{xy}^s\end{Bmatrix},$$
$$\begin{Bmatrix}\gamma_{yz}\\ \gamma_{xz}\end{Bmatrix}=g\begin{Bmatrix}\gamma_{yz}^s\\ \gamma_{xz}^s\end{Bmatrix},\ g=1-\frac{\partial f}{\partial z} \quad (12)$$

where

$$\begin{Bmatrix}\varepsilon_x^0\\ \varepsilon_y^0\\ \gamma_{xy}^0\end{Bmatrix}=\begin{Bmatrix}\frac{\partial u}{\partial x}\\ \frac{\partial v}{\partial y}\\ \frac{\partial u}{\partial y}+\frac{\partial v}{\partial x}\end{Bmatrix},\begin{Bmatrix}\kappa_x^b\\ \kappa_y^b\\ \kappa_{xy}^b\end{Bmatrix}=\begin{Bmatrix}-\frac{\partial^2 w_b}{\partial x^2}\\ -\frac{\partial^2 w_b}{\partial y^2}\\ -2\frac{\partial^2 w_b}{\partial x\partial y}\end{Bmatrix},\begin{Bmatrix}\kappa_x^s\\ \kappa_y^s\\ \kappa_{xy}^s\end{Bmatrix}$$
$$=\begin{Bmatrix}-\frac{\partial^2 w_s}{\partial x^2}\\ -\frac{\partial^2 w_s}{\partial y^2}\\ -2\frac{\partial^2 w_s}{\partial x\partial y}\end{Bmatrix},\begin{Bmatrix}\gamma_{yz}^s\\ \gamma_{xz}^s\end{Bmatrix}=\begin{Bmatrix}\frac{\partial w_s}{\partial y}\\ \frac{\partial w_s}{\partial x}\end{Bmatrix} \quad (13)$$

According to Eq. (10), the relation between electric field (E_x, E_y, E_z) and electric potential (Φ), can be obtained as:

$$E_x=-\Phi_{,x}=\cos(\xi(z))\frac{\partial\phi}{\partial x}, \quad (14)$$

$$E_y=-\Phi_{,y}=\cos(\xi(z))\frac{\partial\phi}{\partial y}, \quad (15)$$

$$E_z=-\Phi_{,z}=-\xi\sin(\xi(z))\phi-\frac{2V}{h} \quad (16)$$

Also, the relation between magnetic field (H_x,H_y,H_z) and magnetic potential (Υ) can be expressed from Eq. (11) as:

$$H_x=-\Upsilon_{,x}=\cos(\xi(z))\frac{\partial\gamma}{\partial x}, \quad (17)$$

$$H_y=-\Upsilon_{,y}=\cos(\xi(z))\frac{\partial\gamma}{\partial y}, \quad (18)$$

$$H_z=-\Upsilon_{,z}=-\xi\sin(\xi(z))\gamma-\frac{2\Omega}{h} \quad (19)$$

Through extended Hamilton's principle, the equation of motion can be derived by:

$$\int_0^t\delta(\Pi_S-\Pi_K+\Pi_W)dt=0 \quad (20)$$

Here Π_S is strain energy, Π_W is work done by external forces and Π_K is kinetic energy. The virtual variation of strain energy can be written as:

$$\delta\Pi_S=\int_v\sigma_{ij}\delta\varepsilon_{ij}\,dV=\int_v(\sigma_x\delta\varepsilon_x+\sigma_y\delta\varepsilon_y+\sigma_{xy}\delta\gamma_{xy}+\sigma_{yz}\delta\gamma_{yz}+\sigma_{xz}\delta\gamma_{xz}$$
$$-D_x\delta E_x-D_y\delta E_y-D_z\delta E_z-B_x\delta H_x-B_y\delta H_y-B_z\delta H_z)\,dV \quad (21)$$

Substituting Eqs. (12) and (13) into Eq. (21) yields

$$\begin{aligned}\delta\Pi_S &= \int_0^L [N_x \frac{\partial\delta u}{\partial x} - M_x^b \frac{\partial^2\delta w_b}{\partial x^2} - M_x^s \frac{\partial^2\delta w_s}{\partial x^2} + N_y \frac{\partial\delta v}{\partial y} - M_y^b \frac{\partial^2\delta w_b}{\partial y^2} - M_y^s \frac{\partial^2\delta w_s}{\partial y^2} \\ &+ N_{xy}(\frac{\partial\delta u}{\partial y} + \frac{\partial\delta v}{\partial x}) - 2M_{xy}^b \frac{\partial^2\delta w_b}{\partial x\partial y} - 2M_{xy}^s \frac{\partial^2\delta w_s}{\partial x\partial y} + Q_{yz} \frac{\partial\delta w_s}{\partial y} + Q_{xz} \frac{\partial\delta w_s}{\partial x}]dx \\ &+ \int_0^L \int_{-h/2}^{h/2} [-D_x \cos(\xi z)\delta\left(\frac{\partial\phi}{\partial x}\right) - D_y \cos(\xi z)\delta\left(\frac{\partial\phi}{\partial y}\right) + D_z \xi \sin(\xi z)\delta\phi \\ &- B_x \cos(\xi z)\delta\left(\frac{\partial\gamma}{\partial x}\right) - B_y \cos(\xi z)\delta\left(\frac{\partial\gamma}{\partial y}\right) + B_z \xi \sin(\xi z)\delta\gamma]dzdx\end{aligned} \tag{22}$$

In which the variables at the last expression are expressed by

$$(N_i, M_i^b, M_i^s) = \int_A (1, z, f)\sigma_i \, dA, \; i = (x, y, xy) \tag{23}$$

$$Q_i = \int_A g\sigma_i \, dA, \; i = (xz, yz) \tag{24}$$

The first variation of work done by applied forces can be written in the form:

$$\begin{aligned}\delta\Pi_W &= \int_0^L (N_x^0 \frac{\partial(w_b + w_s)}{\partial x} \frac{\partial\delta(w_b + w_s)}{\partial x} + N_y^0 \frac{\partial(w_b + w_s)}{\partial y} \frac{\partial\delta(w_b + w_s)}{\partial y} \\ &+ 2\delta N_{xy}^0 \frac{\partial(w_b + w_s)}{\partial x} \frac{\partial(w_b + w_s)}{\partial y} - k_w\delta(w_b + w_s) + k_p \frac{\partial^2(w_b + w_s)}{\partial x^2})dx\end{aligned} \tag{25}$$

where N_x^0, N_y^0, N_{xy}^0 are in-plane applied loads and k_W, k_p are linear and shear coefficient of elastic foundation parameters. The first variational of the virtual kinetic energy of present plate model can be written in the form as

$$\begin{aligned}\delta K &= \int_0^L [I_0(\frac{\partial u}{\partial t}\frac{\partial\delta u}{\partial t} + \frac{\partial v}{\partial t}\frac{\partial\delta v}{\partial t} + \frac{\partial(w_b + w_s)}{\partial t}\frac{\partial\delta(w_b + w_s)}{\partial t}) \\ &- I_1(\frac{\partial u}{\partial t}\frac{\partial\delta w_b}{\partial x\partial t} + \frac{\partial w_b}{\partial x\partial t}\frac{\partial\delta u}{\partial t} + \frac{\partial v}{\partial t}\frac{\partial\delta w_b}{\partial y\partial t} \\ &+ \frac{\partial w_b}{\partial y\partial t}\frac{\partial\delta v}{\partial t}) - J_1(\frac{\partial u}{\partial t}\frac{\partial\delta w_s}{\partial x\partial t} + \frac{\partial w_s}{\partial x\partial t}\frac{\partial\delta u}{\partial t} + \frac{\partial v}{\partial t}\frac{\partial\delta w_s}{\partial y\partial t} + \frac{\partial w_s}{\partial y\partial t}\frac{\partial\delta v}{\partial t}) \\ &+ I_2(\frac{\partial w_b}{\partial x\partial t}\frac{\partial\delta w_b}{\partial x\partial t} + \frac{\partial w_b}{\partial y\partial t}\frac{\partial\delta w_b}{\partial y\partial t}) \\ &+ K_2(\frac{\partial w_s}{\partial x\partial t}\frac{\partial\delta w_s}{\partial x\partial t} + \frac{\partial w_s}{\partial y\partial t}\frac{\partial\delta w_s}{\partial y\partial t}) \\ &+ J_2(\frac{\partial w_b}{\partial x\partial t}\frac{\partial\delta w_s}{\partial x\partial t} + \frac{\partial w_s}{\partial x\partial t}\frac{\partial\delta w_b}{\partial x\partial t} + \frac{\partial w_b}{\partial y\partial t}\frac{\partial\delta w_s}{\partial y\partial t} + \frac{\partial w_s}{\partial y\partial t}\frac{\partial\delta w_b}{\partial y\partial t})]dAdx\end{aligned} \tag{26}$$

In which I_0, I_1, J_1, I_2, J_2 and K_2 are mass inertia and defined as

$$\begin{aligned}&(I_0, I_1, J_1, I_2, J_2, K_2) \\ &= \int_{-h/2-C}^{h/2-C} (1, z, f, z^2, z\ f, f^2)\rho dz_{ns}\end{aligned} \tag{27}$$

The following Euler–Lagrange equations are obtained by inserting Eqs. (22), (24) and (26) in Eq. (20) when the coefficients of δu, δv, δw_b, δw_s, $\delta\phi$ and $\delta\gamma$ are equal to zero

$$\frac{\partial N_x}{\partial x} + \frac{\partial N_{xy}}{\partial y} = I_0 \frac{\partial^2 u}{\partial t^2} - I_1 \frac{\partial^3 w_b}{\partial x\partial t^2} - J_1 \frac{\partial^3 w_s}{\partial x\partial t^2} \tag{28}$$

$$\frac{\partial N_{xy}}{\partial x} + \frac{\partial N_y}{\partial y} = I_0 \frac{\partial^2 v}{\partial t^2} - I_1 \frac{\partial^3 w_b}{\partial y\partial t^2} - J_1 \frac{\partial^3 w_s}{\partial y\partial t^2} \tag{29}$$

$$\begin{aligned}&\frac{\partial^2 M_x^b}{\partial x^2} + 2\frac{\partial^2 M_{xy}^b}{\partial x\partial y} + \frac{\partial^2 M_y^b}{\partial y^2} - (N^E + N^H - k_p)\nabla^2(w_b + w_s) \\ &- k_W(w_b + w_s) = I_0 \frac{\partial^2(w_b + w_s)}{\partial t^2} \\ &+ I_1(\frac{\partial^3 u}{\partial x\partial t^2} + \frac{\partial^3 v}{\partial y\partial t^2}) \\ &- I_2\nabla^2(\frac{\partial^2 w_b}{\partial t^2}) - J_2\nabla^2(\frac{\partial^2 w_s}{\partial t^2})\end{aligned} \tag{30}$$

$$\begin{aligned}&\frac{\partial^2 M_x^s}{\partial x^2} + 2\frac{\partial^2 M_{xy}^s}{\partial x\partial y} + \frac{\partial^2 M_y^s}{\partial y^2} + \frac{\partial Q_{xz}}{\partial x} + \frac{\partial Q_{yz}}{\partial y} \\ &- (N^E + N^H - k_p)\nabla^2(w_b + w_s) \\ &- k_W(w_b + w_s) = I_0 \frac{\partial^2(w_b + w_s)}{\partial t^2} \\ &+ J_1(\frac{\partial^3 u}{\partial x\partial t^2} + \frac{\partial^3 v}{\partial y\partial t^2}) - J_2\nabla^2(\frac{\partial^2 w_b}{\partial t^2}) - K_2\nabla^2(\frac{\partial^2 w_s}{\partial t^2})\end{aligned} \tag{31}$$

$$\int_{-h/2}^{h/2}\left(\cos(\xi z)\frac{\partial D_x}{\partial x} + \cos(\xi z)\frac{\partial D_y}{\partial y} + \xi\sin(\xi z)D_z\right)dz = 0 \tag{32}$$

$$\int_{-h/2}^{h/2}\left(\cos(\xi z)\frac{\partial B_x}{\partial x} + \cos(\xi z)\frac{\partial B_y}{\partial y} + \xi\sin(\xi z)B_z\right)dz = 0 \tag{33}$$

For a linear MEE porous FG plate exposed to magneto-electro-mechanical loading, the coupled constitutive relations may be rewritten as

$$\sigma_{ij} = C_{ijkl}\varepsilon_{kl} - e_{mij}E_m - q_{nij}H_n \tag{34}$$

$$D_i = e_{ikl}\varepsilon_{kl} + k_{im}E_m + d_{in}H_n \tag{35}$$

$$B_i = q_{ikl}\varepsilon_{kl} + d_{im}E_m + \chi_{in}H_n \tag{36}$$

which σ_{ij}, D_i, B_i denotes the components of stress, electric displacement and magnetic induction, ε_{kl}, E_m and H_n are the components of linear strain, electric field and magnetic field. Additionally, C_{ijkl}, k_{im} and χ_{in} are the components of elastic stiffness, dielectric permittivity and magnetic permittivity coefficients; Finally, e_{mij} q_{nij} and d_{in} are the piezoelectric, piezo-magnetic, and magneto-electric-elastic coefficients, respectively. Hence, the stress-strain relations can be expressed by

$$\sigma_{xx} = \tilde{c}_{11}\varepsilon_{xx} + \tilde{c}_{12}\varepsilon_{yy} - \tilde{e}_{31}E_z - \tilde{q}_{31}H_z \tag{37}$$

$$\sigma_{yy} = \tilde{c}_{12}\varepsilon_{xx} + \tilde{c}_{11}\varepsilon_{yy} - \tilde{e}_{31}E_z - \tilde{q}_{31}H_z \tag{38}$$

$$\sigma_{xy} = \tilde{c}_{66}\gamma_{xy} \tag{39}$$

$$\sigma_{xz} = \tilde{c}_{55}\gamma_{xz} - \tilde{e}_{15}E_x - \tilde{q}_{15}H_x \tag{40}$$

$$\sigma_{yz} = \tilde{c}_{55}\gamma_{yz} - \tilde{e}_{15}E_y - \tilde{q}_{15}H_y \tag{41}$$

$$D_x = \tilde{e}_{15}\gamma_{xz} + \tilde{k}_{11}E_x + \tilde{d}_{11}H_x \tag{42}$$

$$D_y = \tilde{e}_{15}\gamma_{yz} + \tilde{k}_{11}E_y + \tilde{d}_{11}H_y \tag{43}$$

$$D_z = \tilde{e}_{31}\varepsilon_{xx} + \tilde{e}_{31}\varepsilon_{yy} + \tilde{k}_{33}E_z + \tilde{d}_{33}H_z \tag{44}$$

$$B_x = \tilde{q}_{15}\gamma_{xz} + \tilde{d}_{11}E_x + \tilde{\chi}_{11}H_x \tag{45}$$

$$B_y = \tilde{q}_{15}\gamma_{yz} + \tilde{d}_{11}E_y + \tilde{\chi}_{11}H_y \tag{46}$$

$$B_z = \tilde{q}_{31}\varepsilon_{xx} + \tilde{q}_{31}\varepsilon_{yy} + \tilde{d}_{33}E_z + \tilde{\chi}_{33}H_z \tag{47}$$

where $\tilde{c}_{ij}, \tilde{e}_{ij}, \tilde{q}_{ij}, \tilde{d}_{ij}, \tilde{k}_{ij}$ and $\tilde{\chi}_{ij}$ are reduced constants for the FG plate under the plane stress state [44] which are given as

$$\begin{aligned}
&\tilde{c}_{11} = c_{11} - \frac{c_{13}^2}{c_{33}},\ \tilde{c}_{12} = c_{12} - \frac{c_{13}^2}{c_{33}},\\
&\tilde{c}_{66} = c_{66},\quad \tilde{e}_{15} = e_{15},\quad \tilde{e}_{31} = e_{31} - \frac{c_{13}e_{33}}{c_{33}},\\
&\tilde{q}_{15} = q_{15},\ \tilde{q}_{31} = q_{31} - \frac{c_{13}q_{33}}{c_{33}},\\
&\tilde{d}_{11} = \tilde{d}_{11},\quad \tilde{d}_{33} = \tilde{d}_{33} + \frac{q_{33}e_{33}}{c_{33}},\\
&\tilde{k}_{11} = k_{11},\ \tilde{k}_{33} = k_{33} + \frac{e_{33}^2}{c_{33}},\\
&\tilde{\chi}_{11} = \chi_{11},\quad \tilde{\chi}_{33} = \chi_{33} + \frac{q_{33}^2}{c_{33}}
\end{aligned} \tag{48}$$

By integrating Eq. (37)-(47) over the area of MEE porous FG plate cross-section, the following relations for the force-strain and the moment-strain and other necessary relation of the refined FG plate can be obtained

$$\begin{Bmatrix} N_x \\ N_y \\ N_{xy} \end{Bmatrix} = \begin{pmatrix} A_{11} & A_{12} & 0 \\ A_{12} & A_{22} & 0 \\ 0 & 0 & A_{66} \end{pmatrix} \begin{Bmatrix} \frac{\partial u}{\partial x} \\ \frac{\partial v}{\partial y} \\ \frac{\partial u}{\partial y} + \frac{\partial v}{\partial x} \end{Bmatrix} + \begin{pmatrix} B_{11} & B_{12} & 0 \\ B_{12} & B_{22} & 0 \\ 0 & 0 & B_{66} \end{pmatrix} \begin{Bmatrix} -\frac{\partial^2 w_b}{\partial x^2} \\ -\frac{\partial^2 w_b}{\partial y^2} \\ -2\frac{\partial^2 w_b}{\partial x \partial y} \end{Bmatrix} \tag{49}$$

$$+ \begin{pmatrix} B_{11}^s & B_{12}^s & 0 \\ B_{12}^s & B_{22}^s & 0 \\ 0 & 0 & B_{66}^s \end{pmatrix} \begin{Bmatrix} -\frac{\partial^2 w_s}{\partial x^2} \\ -\frac{\partial^2 w_s}{\partial y^2} \\ -2\frac{\partial^2 w_s}{\partial x \partial y} \end{Bmatrix} + \begin{Bmatrix} A_{31}^e \\ A_{31}^e \\ 0 \end{Bmatrix} \phi + \begin{Bmatrix} A_{31}^m \\ A_{31}^m \\ 0 \end{Bmatrix} \gamma$$

$$\begin{Bmatrix} M_x^b \\ M_y^b \\ M_{xy}^b \end{Bmatrix} = \begin{pmatrix} B_{11} & B_{12} & 0 \\ B_{12} & B_{22} & 0 \\ 0 & 0 & B_{66} \end{pmatrix} \begin{Bmatrix} \frac{\partial u}{\partial x} \\ \frac{\partial v}{\partial y} \\ \frac{\partial u}{\partial y} + \frac{\partial v}{\partial x} \end{Bmatrix} + \begin{pmatrix} D_{11} & D_{12} & 0 \\ D_{12} & D_{22} & 0 \\ 0 & 0 & D_{66} \end{pmatrix} \begin{Bmatrix} -\frac{\partial^2 w_b}{\partial x^2} \\ -\frac{\partial^2 w_b}{\partial y^2} \\ -2\frac{\partial^2 w_b}{\partial x \partial y} \end{Bmatrix} \tag{50}$$

$$+ \begin{pmatrix} D_{11}^s & D_{12}^s & 0 \\ D_{12}^s & D_{22}^s & 0 \\ 0 & 0 & D_{66}^s \end{pmatrix} \begin{Bmatrix} -\frac{\partial^2 w_s}{\partial x^2} \\ -\frac{\partial^2 w_s}{\partial y^2} \\ -2\frac{\partial^2 w_s}{\partial x \partial y} \end{Bmatrix} + \begin{Bmatrix} E_{31}^e \\ E_{31}^e \\ 0 \end{Bmatrix} \phi + \begin{Bmatrix} E_{31}^m \\ E_{31}^m \\ 0 \end{Bmatrix} \gamma$$

$$\begin{Bmatrix} M_x^s \\ M_y^s \\ M_{xy}^s \end{Bmatrix} = \begin{pmatrix} B_{11}^s & B_{12}^s & 0 \\ B_{12}^s & B_{22}^s & 0 \\ 0 & 0 & B_{66}^s \end{pmatrix} \begin{Bmatrix} \frac{\partial u}{\partial x} \\ \frac{\partial v}{\partial y} \\ \frac{\partial u}{\partial y} + \frac{\partial v}{\partial x} \end{Bmatrix} + \begin{pmatrix} D_{11}^s & D_{12}^s & 0 \\ D_{12}^s & D_{22}^s & 0 \\ 0 & 0 & D_{66}^s \end{pmatrix} \begin{Bmatrix} -\frac{\partial^2 w_b}{\partial x^2} \\ -\frac{\partial^2 w_b}{\partial y^2} \\ -2\frac{\partial^2 w_b}{\partial x \partial y} \end{Bmatrix} \tag{51}$$

$$+ \begin{pmatrix} H_{11}^s & H_{12}^s & 0 \\ H_{12}^s & H_{22}^s & 0 \\ 0 & 0 & H_{66}^s \end{pmatrix} \begin{Bmatrix} -\frac{\partial^2 w_s}{\partial x^2} \\ -\frac{\partial^2 w_s}{\partial y^2} \\ -2\frac{\partial^2 w_s}{\partial x \partial y} \end{Bmatrix} + \begin{Bmatrix} F_{31}^e \\ F_{31}^e \\ 0 \end{Bmatrix} \phi + \begin{Bmatrix} F_{31}^m \\ F_{31}^m \\ 0 \end{Bmatrix} \gamma$$

$$\begin{Bmatrix} Q_{xz} \\ Q_{yz} \end{Bmatrix} = \begin{pmatrix} A_{44}^s & 0 \\ 0 & A_{55}^s \end{pmatrix} \begin{Bmatrix} \frac{\partial w_s}{\partial x} \\ \frac{\partial w_s}{\partial y} \end{Bmatrix} - A_{15}^e \begin{Bmatrix} \frac{\partial \phi}{\partial x} \\ \frac{\partial \phi}{\partial y} \end{Bmatrix} - A_{15}^m \begin{Bmatrix} \frac{\partial \gamma}{\partial x} \\ \frac{\partial \gamma}{\partial y} \end{Bmatrix} \tag{52}$$

$$\int_{-h/2}^{h/2} \begin{Bmatrix} D_x \\ D_y \end{Bmatrix} \cos(\xi z) dz = E_{15}^e \begin{Bmatrix} \frac{\partial w_s}{\partial x} \\ \frac{\partial w_s}{\partial y} \end{Bmatrix} + F_{11}^e \begin{Bmatrix} \frac{\partial \phi}{\partial x} \\ \frac{\partial \phi}{\partial y} \end{Bmatrix} + F_{11}^m \begin{Bmatrix} \frac{\partial \gamma}{\partial x} \\ \frac{\partial \gamma}{\partial y} \end{Bmatrix} \tag{53}$$

$$\begin{aligned}
&\int_{-h/2}^{h/2} D_z\, \xi \sin(\xi z) dz = A_{31}^e \left(\frac{\partial u}{\partial x} + \frac{\partial v}{\partial y}\right)\\
&-E_{31}^e \nabla^2 w_b - F_{31}^e \nabla^2 w_s - F_{33}^e \phi - F_{33}^m \gamma
\end{aligned} \tag{54}$$

$$\int_{-h/2}^{h/2} \begin{Bmatrix} B_x \\ B_y \end{Bmatrix} \cos(\xi z) dz = E_{15}^m \begin{Bmatrix} \frac{\partial w_s}{\partial x} \\ \frac{\partial w_s}{\partial y} \end{Bmatrix} + F_{11}^m \begin{Bmatrix} \frac{\partial \phi}{\partial x} \\ \frac{\partial \phi}{\partial y} \end{Bmatrix} + X_{11}^m \begin{Bmatrix} \frac{\partial \gamma}{\partial x} \\ \frac{\partial \gamma}{\partial y} \end{Bmatrix} \tag{55}$$

$$\begin{aligned}
&\int_{-h/2}^{h/2} B_z\, \xi \sin(\xi z) dz = A_{31}^m \left(\frac{\partial u}{\partial x} + \frac{\partial v}{\partial y}\right)\\
&-E_{31}^m \nabla^2 w_b - F_{31}^m \nabla^2 w_s - F_{33}^m \phi - X_{33}^m \gamma
\end{aligned} \tag{56}$$

In which the cross-sectional rigidities are defined as follows

$$\begin{Bmatrix} A_{11}, B_{11}, B_{11}^s, D_{11}, D_{11}^s, H_{11}^s \\ A_{12}, B_{12}, B_{12}^s, D_{12}, D_{12}^s, H_{12}^s \\ A_{66}, B_{66}, B_{66}^s, D_{66}, D_{66}^s, H_{66}^s \end{Bmatrix} = \int_{-h/2-C}^{h/2-C} \begin{Bmatrix} \tilde{c}_{11} \\ \tilde{c}_{12} \\ \tilde{c}_{66} \end{Bmatrix} (1, z, f, z^2, z\ f, f^2) dz \tag{57}$$

$$\left\{A_{31}^e, E_{31}^e, F_{31}^e\right\} = \int_{-h/2}^{h/2} \tilde{e}_{31} \xi \sin(\xi z) \left\{1, z, f\right\} dz \tag{58}$$

$$\left\{A_{31}^m, E_{31}^m, F_{31}^m\right\} = \int_{-h/2}^{h/2} \tilde{q}_{31} \xi \sin(\xi z) \left\{1, z, f\right\} dz \tag{59}$$

$$\left\{A_{15}^e, E_{15}^e\right\} = \int_{-h/2}^{h/2} \tilde{e}_{15} \cos(\xi z) \left\{1, g\right\} dz \tag{60}$$

$$\left\{A_{15}^m, E_{15}^m\right\} = \int_{-h/2}^{h/2} \tilde{q}_{15} \cos(\xi z) \left\{1, g\right\} dz \tag{61}$$

$$\left\{F_{11}^e, F_{33}^e\right\} = \int_{-h/2}^{h/2} \left\{\tilde{k}_{11} \cos^2(\xi z), \tilde{k}_{33} \xi^2 \sin^2(\xi z)\right\} dz \tag{62}$$

$$\left\{F_{11}^m, F_{33}^m\right\} = \int_{-h/2}^{h/2} \left\{\tilde{d}_{11} \cos^2(\xi z), \tilde{d}_{33} \xi^2 \sin^2(\xi z)\right\} dz \tag{63}$$

$$\left\{X_{11}^m, X_{33}^m\right\} = \int_{-h/2}^{h/2} \left\{\tilde{\chi}_{11} \cos^2(\xi z), \tilde{\chi}_{33} \xi^2 \sin^2(\xi z)\right\} dz \tag{64}$$

$$A_{44}^s = A_{55}^s = \int_{-h/2}^{h/2} \tilde{c}_{55} g^2 dz \tag{65}$$

The governing equations of refined four-variable shear deformation MEE porous FG plate in terms of the displacement can be derived by substituting Eqs. (49) -(56), into Eqs. (28) -(33) as follows:

$$\begin{aligned} &A_{11} \frac{\partial^2 u}{\partial x^2} + A_{66} \frac{\partial^2 u}{\partial y^2} + (A_{12} + A_{66}) \frac{\partial^2 v}{\partial x \partial y} \\ &-B_{11} \frac{\partial^3 w_b}{\partial x^3} - (B_{12} + 2B_{66}) \frac{\partial^3 w_b}{\partial x \partial y^2} - B_{11}^s \frac{\partial^3 w_s}{\partial x^3} \\ &-(B_{12}^s + 2B_{66}^s) \frac{\partial^3 w_s}{\partial x \partial y^2} + A_{31}^e \frac{\partial \phi}{\partial x} \\ &+A_{31}^m \frac{\partial \gamma}{\partial x} - I_0 \frac{\partial^2 u}{\partial t^2} + I_1 \frac{\partial^3 w_b}{\partial x \partial t^2} + J_1 \frac{\partial^3 w_s}{\partial x \partial t^2} = 0 \end{aligned} \tag{66}$$

$$\begin{aligned} &A_{66} \frac{\partial^2 v}{\partial x^2} + A_{22} \frac{\partial^2 v}{\partial y^2} + (A_{12} + A_{66}) \frac{\partial^2 u}{\partial x \partial y} \\ &-B_{22} \frac{\partial^3 w_b}{\partial y^3} - (B_{12} + 2B_{66}) \frac{\partial^3 w_b}{\partial x^2 \partial y} - B_{22}^s \frac{\partial^3 w_s}{\partial y^3} \\ &-(B_{12}^s + 2B_{66}^s) \frac{\partial^3 w_s}{\partial x^2 \partial y} + A_{31}^e \frac{\partial \phi}{\partial y} \\ &+A_{31}^m \frac{\partial \gamma}{\partial y} + I_0 \frac{\partial^2 v}{\partial t^2} - I_1 \frac{\partial^3 w_b}{\partial y \partial t^2} - J_1 \frac{\partial^3 w_s}{\partial y \partial t^2} = 0 \end{aligned} \tag{67}$$

$$\begin{aligned} &B_{11} \frac{\partial^3 u}{\partial x^3} + (B_{12} + 2B_{66}) \frac{\partial^3 u}{\partial x \partial y^2} + (B_{12} + 2B_{66}) \frac{\partial^3 v}{\partial x^2 \partial y} \\ &+B_{22} \frac{\partial^3 v}{\partial y^3} - D_{11} \frac{\partial^4 w_b}{\partial x^4} + E_{31}^e \nabla^2 \phi \\ &-2(D_{12} + 2D_{66}) \frac{\partial^4 w_b}{\partial x^2 \partial y^2} - D_{22} \frac{\partial^4 w_b}{\partial y^4} \\ &-D_{11}^s \frac{\partial^4 w_s}{\partial x^4} - 2(D_{12}^s + 2D_{66}^s) \frac{\partial^4 w_s}{\partial x^2 \partial y^2} + E_{31}^m \nabla^2 \gamma \\ &-D_{22}^s \frac{\partial^4 w_s}{\partial y^4} + I_0 \frac{\partial^2 (w_b + w_s)}{\partial t^2} \\ &+I_1 \left(\frac{\partial^3 u}{\partial x \partial t^2} + \frac{\partial^3 v}{\partial y \partial t^2}\right) - I_2 \nabla^2 \left(\frac{\partial^2 w_b}{\partial t^2}\right) - J_2 \nabla^2 \left(\frac{\partial^2 w_s}{\partial t^2}\right) \\ &-(N^E + N^H - k_p) \nabla^2 (w_b + w_s) - k_W (w_b + w_s) = 0 \end{aligned} \tag{68}$$

$$\begin{aligned} &B_{11}^s \frac{\partial^3 u}{\partial x^3} + (B_{12}^s + 2B_{66}^s) \frac{\partial^3 u}{\partial x \partial y^2} + (B_{12}^s + 2B_{66}^s) \frac{\partial^3 v}{\partial x^2 \partial y} \\ &+B_{22}^s \frac{\partial^3 v}{\partial y^3} - D_{11}^s \frac{\partial^4 w_b}{\partial x^4} + A_{55}^s \frac{\partial^2 w_s}{\partial x^2} \\ &+A_{44}^s \frac{\partial^2 w_s}{\partial y^2} - 2(D_{12}^s + 2D_{66}^s) \frac{\partial^4 w_b}{\partial x^2 \partial y^2} \\ &-D_{22}^s \frac{\partial^4 w_b}{\partial y^4} - H_{11}^s \frac{\partial^4 w_s}{\partial x^4} - 2(H_{12}^s + 2H_{66}^s) \frac{\partial^4 w_s}{\partial x^2 \partial y^2} \\ &-H_{22}^s \frac{\partial^4 w_s}{\partial y^4} + F_{31}^e \nabla^2 \phi + F_{31}^m \nabla^2 \gamma \\ &+I_0 \frac{\partial^2 (w_b + w_s)}{\partial t^2} + J_1 \left(\frac{\partial^3 u}{\partial x \partial t^2} + \frac{\partial^3 v}{\partial y \partial t^2}\right) - J_2 \nabla^2 \left(\frac{\partial^2 w_b}{\partial t^2}\right) \\ &-K_2 \nabla^2 \left(\frac{\partial^2 w_s}{\partial t^2}\right) - (N^E + N^H - k_p) \nabla^2 (w_b + w_s) \\ &-k_W (w_b + w_s) - A_{15}^e \nabla^2 \phi - A_{15}^m \nabla^2 \gamma = 0 \end{aligned} \tag{69}$$

$$\begin{aligned} &A_{31}^e \left(\frac{\partial u}{\partial x} + \frac{\partial v}{\partial y}\right) - E_{31}^e \nabla^2 w_b - F_{31}^e \nabla^2 w_s \\ &+E_{15}^e \nabla^2 w_s + F_{11}^e \nabla^2 \phi + F_{11}^m \nabla^2 \gamma - F_{33}^e \phi - F_{33}^m \gamma = 0 \end{aligned} \tag{70}$$

$$\begin{aligned} &A_{31}^m \left(\frac{\partial u}{\partial x} + \frac{\partial v}{\partial y}\right) - E_{31}^m \nabla^2 w_b - F_{31}^m \nabla^2 w_s \\ &+E_{15}^m \nabla^2 w_s + F_{11}^m \nabla^2 \phi + X_{11}^m \nabla^2 \gamma - F_{33}^m \phi - X_{33}^m \gamma = 0 \end{aligned} \tag{71}$$

In this study it assumed that the porous MEE-FG plate is under external electric voltage, magnetic potential and the shear loading is ignored. So $N_{xy}^0 = 0$ and N_x^0, N_y^0 are the normal forces induced by external electric voltage V and external magnetic potential Ω, respectively and are defined as

$$N_x^0 = N_y^0 = N^E + N^H$$

$$N^E = -\int_{-h/2}^{h/2} \tilde{e}_{31} \frac{2V}{h} dz, N^H = -\int_{-h/2}^{h/2} \tilde{q}_{31} \frac{2\Omega}{h} dz \tag{72}$$

3. Solution procedure

Here, an exact solution of the governing equations for free vibration of a MEE porous FG plate with simply-supported (S), clamped (C) or free (F) edges or combinations of these boundary conditions is presented which they are given as

- Simply-supported (S)

$$w_b = w_s = N_x = M_x = 0 \quad \text{at x=0,a}$$
$$w_b = w_s = N_y = M_y = 0 \quad \text{at y=0,b} \tag{73}$$

- Clamped (C)

$$u = v = w_b = w_s = 0 \quad \text{at x=0,a and y=0,b} \tag{74}$$

- Free (F)

$$M_x = M_{xy} = Q_{xz} = 0 \quad \text{at x=0,a}$$
$$M_y = M_{xy} = Q_{yz} = 0 \quad \text{at y=0,b} \tag{75}$$

To satisfy above-mentioned boundary conditions, the displacement quantities are presented in the following form:

$$u = \sum_{m=1}^{\infty}\sum_{n=1}^{\infty} U_{mn} \frac{\partial X_m(x)}{\partial x} Y_n(y) e^{i\omega_n t} \tag{76}$$

$$w_b = \sum_{m=1}^{\infty}\sum_{n=1}^{\infty} W_{bmn} X_m(x) Y_n(y) e^{i\omega_n t} \tag{77}$$

$$v = \sum_{m=1}^{\infty}\sum_{n=1}^{\infty} V_{mn} X_m(x) \frac{\partial Y_n(y)}{\partial y} e^{i\omega_n t} \tag{78}$$

$$w_s = \sum_{m=1}^{\infty}\sum_{n=1}^{\infty} W_{smn} X_m(x) Y_n(y) e^{i\omega_n t} \tag{79}$$

$$\phi = \sum_{m=1}^{\infty}\sum_{n=1}^{\infty} \Phi_{mn} X_m(x) Y_n(y) e^{i\omega_n t} \tag{80}$$

$$\gamma = \sum_{m=1}^{\infty}\sum_{n=1}^{\infty} \gamma_{mn} X_m(x) Y_n(y) e^{i\omega_n t} \tag{81}$$

where (U_{mn}, V_{mn}, W_{bmn} W_{smn}, W_{smn}, Φ_{mn}, γ_{mn}) are the unknown coefficients and the functions X_m and Y_n are tabulated in detail in Table 2 for different boundary conditions ($\alpha=m\pi/a$, $\beta=n\pi/b$). Inserting Eqs. (76)-(81) into Eqs. (66)-(71) respectively, leads to

$$\begin{aligned}&[\left(A_{11}r_1 + A_{66}r_2\right) + I_0\omega_n^2(r_{11})]U_{mn} + \left(A_{12} + A_{66}\right)r_2 V_{mn}\\ &-[B_{11}r_1 + \left(B_{12} + 2B_{66}\right)r_2 + I_1\omega_n^2 r_{11}]W_{bmn}\\ &+[-\left(B_{12}^s + 2B_{66}^s\right)r_2 - B_{11}^s r_1 + J_1\omega_n^2(-r_{11})]W_{smn}\\ &+A_{31}^e r_{11}\psi_{mn} + A_{31}^m r_{11}\gamma_{mn} = 0\end{aligned} \tag{83}$$

$$\begin{aligned}&[(A_{12} + A_{66})r_3]U_{mn} + [A_{66}r_3 + A_{22}r_4 + I_0\omega_n^2(r_{12})]V_{mn}\\ &+[-B_{22}r_4 - (B_{12} + 2B_{66})r_3 - I_1\omega_n^2(r_{12})]W_{bmn}\\ &+[-B_{22}^s r_4 - (B_{12}^s + 2B_{66}^s)r_1 - J_1\omega_n^2(r_{12})]W_{smn}\\ &+A_{31}^e r_{12}\psi_{mn} + A_{31}^m r_{12}\lambda_{mn} = 0\end{aligned} \tag{84}$$

$$\begin{aligned}&[B_{11}r_5 + (B_{12} + 2B_{66})r_6 + I_1\omega_n^2(-r_{10})]U_{mn}\\ &+[(B_{12} + 2B_{66})r_6 + B_{22}r_7 + I_1\omega_n^2(r_9)]V_{mn}\\ &+[-D_{11}r_5 - 2(D_{12} + 2D_{66})r_6 - D_{22}r_7 - I_2\omega_n^2((r_{10} + r_9))\\ &-I_0\omega_n^2(-r_8) + (N^E + N^H - k_p)(-(r_{10} + r_9))]W_{bmn}\\ &+[-D_{11}^s r_5 - 2(D_{12}^s + 2D_{66}^s)r_6 - D_{22}^s r_7 - I_0\omega_n^2(-r_8)\\ &+J_2\omega_n^2((r_{10} + r_9)) + (N^E + N^H - k_p)(-(r_{10} + r_9))]W_{smn}\\ &+[E_{31}^e(r_{10} + r_9)]\psi_{mn} + [E_{31}^m(r_9 + r_{10})]\gamma_{mn} = 0\end{aligned} \tag{85}$$

$$\begin{aligned}&[B_{11}^s r_5 + (B_{12}^s + 2B_{66}^s)r_6 + J_1\omega_n^2(-r_{10})]U_{mn}\\ &+[(B_{12}^s + 2B_{66}^s)r_6 + B_{22}^s r_7 + J_1\omega_n^2(+r_9)]V_{mn} + [-D_{11}^s r_5\\ &-2(D_{12}^s + 2D_{66}^s)r_6 - D_{22}^s r_7 - J_2\omega_n^2((r_{10} + r_9))\\ &-I_0\omega_n^2(-r_8) + (N^E + N^H - k_p)(-(r_{10} + r_9))]W_{bmn}\\ &+[A_{44}^s(r_{10} + r_9) - H_{11}^s r_5 - 2(H_{12}^s + 2H_{66}^s)r_6\\ &-H_{22}^s r_7 + (N^E + N^H - k_p)(-(r_{10} + r_9)) - I_0\omega_n^2(-r_8)\\ &-K_2\omega_n^2(r_{10} + r_9)]W_{smn} + [(F_{31}^e - A_{15}^e)(r_{10} + r_9)]\psi_{mn}\\ &+(F_{31}^m - A_{15}^m)(r_{10} + r_9)\gamma_{mn} = 0\end{aligned} \tag{86}$$

$$\begin{aligned}&A_{31}^e r_{10}U_{mn} + A_{31}^e r_9 V_{mn} + [-E_{31}^e(r_{10} + r_9)]W_{bmn}\\ &+[(E_{15}^e - F_{31}^e)(r_{10} + r_9)]W_{smn} + [F_{11}^e(r_{10} + r_9)\\ &-F_{33}^e r_8]\psi_{mn} + [F_{11}^m(r_{10} + r_9) - F_{33}^m r_8]\gamma_{mn} = 0\end{aligned} \tag{87}$$

Table 2 The admissible functions $X_m(x)$ and $Y_n(y)$(Sobhy, 2013)

	Boundary conditions		The functions X_m and Y_n	
	At x=0, a	At y=0, b	$X_m(x)$	$Y_n(y)$
SSSS	$X_m(0)=X_m''(0)=0$	$Y_n(0)=Y_n''(0)=0$	$Sin(\alpha x)$	$Sin(\beta y)$
	$X_m(a)=X_m''(a)=0$	$Y_n(b)=Y_n''(b)=0$		
CSSS	$X_m(0)=X_m'(0)=0$	$Y_n(0)=Y_n''(0)=0$	$Sin(\alpha x)[Cos(\alpha x)-1]$	$Sin(\beta y)$
	$X_m(a)=X_m''(a)=0$	$Y_n(b)=Y_n''(b)=0$		
CSCS	$X_m(0)=X_m'(0)=0$	$Y_n(0)=Y_n'(0)=0$	$Sin(\alpha x)[Cos(\alpha x)-1]$	$Sin(\beta y)[Cos(\beta y)-1]$
	$X_m(a)=X_m''(a)=0$	$Y_n(b)=Y_n''(b)=0$		
CCSS	$X_m(0)=X_m'(0)=0$	$Y_n(0)=Y_n''(0)=0$	$Sin^2(\alpha x)$	$\mathrm{Sin}(\beta y)$
	$\mathrm{X_m(a)=X_m'(a)=0}$	$\mathrm{Y_n(b)=Y_n''(b)=0}$		
CCCC	$\mathrm{X_m(0)=X_m'(0)=0}$	$\mathrm{Y_n(0)=Y_n'(0)=0}$	$\mathrm{Sin^2(\alpha x)}$	$\mathrm{Sin^2(\beta y)}$
	$\mathrm{X_m(a)=X_m'(a)=0}$	$\mathrm{Y_n(b)=Y_n'(b)=0}$		
CCFF	$\mathrm{X_m''(0)=X_m'''(0)=0}$	$\mathrm{Y_n(0)=Y_n'(0)=0}$	$\mathrm{Cos^2(\alpha x)[Sin^2(\alpha x)+1]}$	$\mathrm{Sin^2(\beta y)}$
	$\mathrm{X_m''(a)=X_m'''(a)=0}$	$\mathrm{Y_n(b)=Y_n'(b)=0}$		

$$A_{31}^m r_{10}U_{mn}+A_{31}^m r_9 V_{mn}-E_{31}^m(r_{10}+r_9)W_{bmn}$$
$$+(E_{15}^m-F_{31}^m)(r_{10}+r_9)W_{smn}+[F_{11}^m(r_{10}+r_9)$$
$$-F_{33}^m r_8]\psi_{mn}+[X_{11}^m(r_{10}+r_9)-X_{33}^m r_8]\gamma_{mn}=0 \quad (88)$$

where

$$\{r_3,r_4,r_{12}\}=\int_0^a\int_0^b X(x)Y'(y)\{X''(x)Y'(y),X(x)Y'''(y),X(x)Y'(y)\}dxdy \quad (89)$$

$$\{r_1,r_2,r_{11}\}=\int_0^a\int_0^b X'(x)Y(y)\{X''(x)Y(y),X'(x)Y''(y),X'(x)Y(y)\}dxdy \quad (90)$$

$$\{r_5,r_6,r_7\}=\int_0^a\int_0^b X(x)Y(y)\{X''''(x)Y(y),X''(x)Y''(y),X(x)Y''''(y)\}dxdy \quad (91)$$

$$\{r_8,r_9,r_{10}\}=\int_0^a\int_0^b X(x)Y(y)\{X(x)Y(y),X(x)Y''(y),X''(x)Y(y)\}dxdy \quad (92)$$

By finding determinant of the coefficient matrix of the following equations and setting this multinomial to zero, we can find natural frequencies ω_n.

$$\begin{bmatrix} k_{11} & k_{12} & k_{13} & k_{14} & k_{15} & k_{16} \\ k_{21} & k_{22} & k_{23} & k_{24} & k_{25} & k_{26} \\ k_{31} & k_{32} & k_{33} & k_{34} & k_{35} & k_{36} \\ k_{41} & k_{42} & k_{43} & k_{44} & k_{45} & k_{46} \\ k_{51} & k_{52} & k_{53} & k_{54} & k_{15} & k_{56} \\ k_{61} & k_{62} & k_{63} & k_{64} & k_{65} & k_{66} \end{bmatrix} - \omega^2 \begin{bmatrix} M_{11} & M_{12} & M_{13} & M_{14} & M_{15} & M_{16} \\ M_{21} & M_{22} & M_{23} & M_{24} & M_{25} & M_{26} \\ M_{31} & M_{32} & M_{33} & M_{34} & M_{35} & M_{36} \\ M_{41} & M_{42} & M_{43} & M_{44} & M_{45} & M_{46} \\ M_{51} & M_{52} & M_{53} & M_{54} & M_{15} & M_{56} \\ M_{61} & M_{62} & M_{63} & M_{64} & M_{65} & M_{66} \end{bmatrix} \begin{bmatrix} U_{mn} \\ V_{mn} \\ W_{bmn} \\ W_{smn} \\ \psi_{mn} \\ \gamma_{mn} \end{bmatrix} = 0 \quad (93)$$

4. Numerical results and discussions

Through this section, the proposed model is verified by comparing the obtained results with those of perfect FGM plates presented by Thai and Choi (2012), as illustrated in Table 3. Further, the influence of elastic foundation parameters, porosity volume fraction, FG material gradation, magnetic and electric fields, different types of porosity distributions, various boundary conditions and side to thickness ratio on the natural frequencies of the MEE porous FG plate are evaluated. The non-dimensional natural frequency (λ) can be calculated by the relation in Eq. (94) as

Table 3 Comparison of non-dimensional natural frequency $\hat{\omega}=\omega h\sqrt{\rho_m/E_m}$ of perfect FGM plates for various power-law exponents (a=b=20h)

B.C.		Power-law exponent				
		p=0	p=0.5	p=1	p=2	p=5
SSSS	TPT (Thai and Choi 2012)	0.0291	0.0247	0.0222	0.0202	0.0191
	Present tangential-exponential	0.029153	0.02470	0.022264	0.020241	0.019178
CCSS	TPT (Thai and Choi 2012)	0.0424	0.0359	0.0324	0.0294	0.0278
	Present tangential-exponential	0.043543	0.036905	0.033273	0.03025	0.028639

Table 4 Variation of the non-dimensional frequency of MEE-FG plate with different foundation parameter and porosity distribution under various boundary conditions (a/h=100, Ω=0)

		$\alpha=0.2, V=500$					
		k_w=0, k_p=0			k_w=10, k_p=10		
B.C	Type of FGM	p=0.2	p=1	p=5	p=0.2	p=1	p=5
SSSS	FGM1	4.41499	4.08636	3.83084	16.6333	16.2548	15.9136
	FGM2	4.5017	4.21842	3.99576	15.7441	15.4211	15.1288
CSSS	FGM1	6.31798	5.85629	5.50443	19.2486	18.7743	18.3567
	FGM2	6.44088	6.04276	5.73379	17.5098	17.87	17.5098
CCSS	FGM1	6.61037	6.11364	5.74164	18.484	18.0043	17.5889
	FGM2	6.73481	6.30611	5.98121	17.5803	17.1662	16.8064
CCCC	FGM1	8.30507	7.68116	7.21846	20.1921	19.6222	19.1401
	FGM2	8.45967	7.92106	7.5167	19.271	18.7762	18.3561
CCFF	FGM1	8.84641	8.17373	7.67913	19.9991	19.402	19.9049
	FGM2	9.00846	8.42752	7.99505	19.1278	18.6076	18.1729

$$\lambda=\omega\frac{a^2}{h}\sqrt{\frac{\rho_u}{c_{11u}}} \quad (94)$$

Table 5 Effect of porosity volume fraction and magnetic potential on the non-dimensional frequency of embedded MEE-FG

B.C	Ω	Even porosity ($\frac{a}{h}=100, V=0, k_p=k_w=0$)					
		$\alpha=0$			$\alpha=0.2$		
		p=0.2	p=1	p=5	p=0.2	p=1	p=5
SSSS	-500	3.29439	3.45350	3.75404	3.27061	3.46440	3.86939
	0	4.38393	4.16473	3.99715	4.42483	4.14321	3.92956
	500	5.25511	4.77109	4.22631	5.33491	4.72550	3.86939
CSSS	-500	5.32542	5.31110	5.47088	5.33702	5.30955	5.53937
	0	6.26380	5.93728	5.69035	6.32693	5.90799	5.59416
	500	7.07886	6.50344	5.90167	7.18166	6.45115	5.64842
CCSS	-500	5.75232	5.65300	5.73029	5.78241	5.64781	5.77172
	0	6.54592	6.18688	5.91901	6.61805	6.15812	5.81896
	500	7.25320	6.67823	6.10189	7.3594	6.62926	5.86581
CCCC	-500	7.50850	7.27597	7.24272	7.56624	7.26215	7.24582
	0	8.21775	7.75653	7.41413	8.31205	7.72166	7.28887
	500	8.87047	8.20901	7.58168	8.99625	8.15531	7.33166
CCFF	-500	8.12166	7.81959	7.72228	8.12166	7.81959	7.72228
	0	8.74729	8.24577	7.87495	8.74829	8.24577	7.87495
	500	9.33295	8.65098	8.02471	9.33295	8.65098	8.02471
Uneven porosity							
B.C	Ω	$\alpha=0$			$\alpha=0.2$		
		p=0.2	p=1	p=5	p=0.2	p=1	p=5
SSSS	-500	3.29439	3.4535	3.75404	3.43608	3.59537	3.93172
	0	4.38393	4.16473	3.99715	4.51689	4.27447	4.0881
	500	5.25511	4.77109	4.22631	5.38498	4.85984	4.23871
CSSS	-500	5.32542	5.3111	5.47088	5.52171	5.49421	5.67797
	0	6.2638	5.93728	5.69035	6.45469	6.09373	5.81976
	500	7.07886	6.50344	5.90167	7.2689	6.63933	5.95818
CCSS	-500	5.75232	5.653	5.73029	7.45289	6.82326	6.17323
	0	6.54592	6.18688	5.91901	6.74667	6.34997	6.05357
	500	7.2532	6.67823	6.10189	5.95731	5.83844	5.93149
CCCC	-500	7.5085	7.27597	7.24272	7.76456	7.50016	7.47154
	0	8.21775	7.75653	7.41413	8.47046	7.96100	7.58261
	500	8.87047	8.20901	7.58168	9.12189	8.3966	7.69208
CCFF	-500	8.12166	7.81959	7.72228	8.39427	8.05427	7.95483
	0	8.74729	8.24577	7.87495	9.01806	8.46312	8.05382
	500	9.33295	8.65098	8.02471	9.60141	8.85311	8.15161

In Table 4, the effect of elastic foundation stiffness, porosity distribution and material gradation exponent on the non-dimensional frequency of the MEE-porous FG plates resting on two-parameter elastic foundation are listed for various boundary conditions (SSSS, CSSS, CCSS, CCCC and CCFF), elastic foundation (k_w=0, 10, k_p=0, 10), power-law indexes (p = 0.2,1,5) and two porosity distributions (even, uneven) at (a/h=100, V=+500, Ω=0, α=0.2).

Also table 5 present the non-dimensional frequency of MEE-porous FG plates resting on elastic foundation for different boundary conditions (SSSS, CSSS, CCSS, CCCC and CCFF), magnetic potentials (Ω=-500, 0, +500), power-law indexes (p=0.2,1,5), porosity volume fraction (α=0, α=0.2) and two porosity distributions (even, uneven) at (a/h=100, V=+500, k_w=0, k_p=0).

Form the results of these tables, it is concluded that increasing the power-law exponents leads to the reduction in the non-dimensional frequency of both porosity distributions. In fact, when p = 0, the plate is completely composed of $CoFe_2O_4$ and has the greatest frequency. Increasing the material gradation exponent from 0 to 10changes the composition of the MEE-FG plate from a fully $CoFe_2O_4$ plate to a plate with a combination of $CoFe_2O_4$ and $BaTiO_3$.Therefore, by increasing the metal percentage results in the lower value of Young's modulus of $BaTiO_3$ with respect to $CoFe_2O_4$. Therefore, the stiffness of

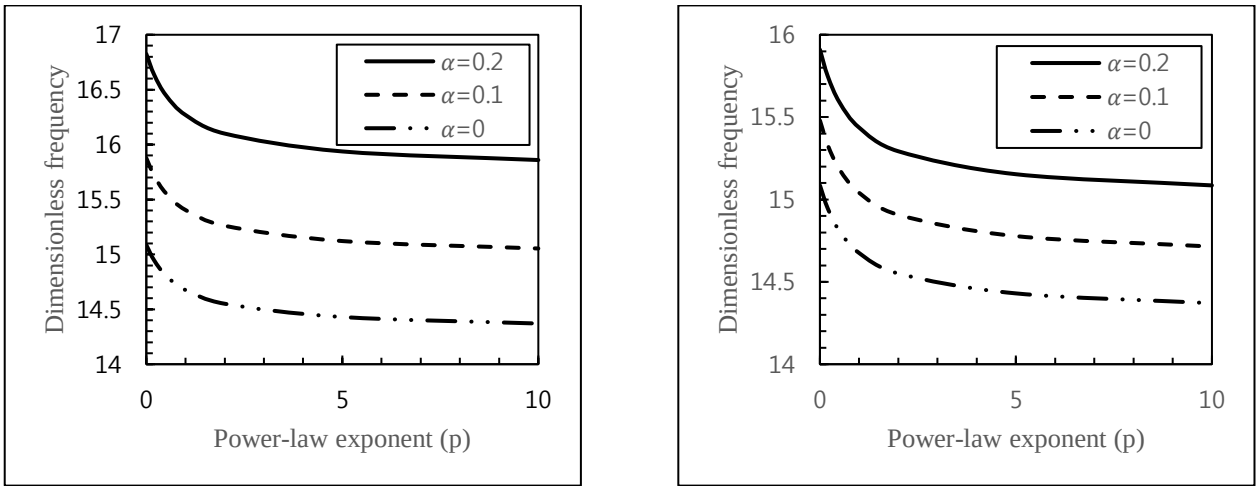

(a) Even porosity (k_w=0, k_p=0) (b) Uneven porosity (k_w=10, k_p=10)

Fig. 3. The variation of the first dimensionless frequency of SSSS MEE-FGM(I) &(II) plate resting on elastic foundations with material graduation and porosity parameter (a/h=100, Ω=0, V=0)

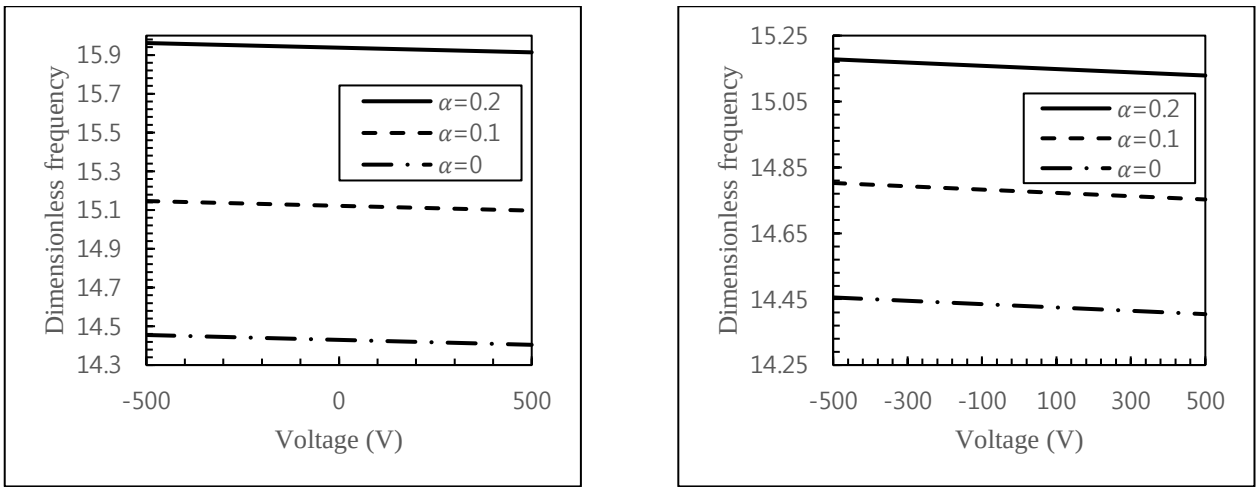

(a) even porosity (b) uneven porosity

Fig. 4. Effect of porosity volume index on the dimensionless frequency of the SSSS MEE-FGM(I) plate on elastic foundations with respect to applied electric voltage (a/h=100, Ω=0 p = 5, k_w = 10, k_p = 10).

system and in turn the natural frequency of the structure diminishes. In addition, it can be witnessed that the elastic foundations tends to increase the non-dimensional frequency of MEE-porous FG plate. Also it is found that the effect of the magnetic field depends on the sign of magnetic potential, in other words negative values of magnetic potential leads to decrease the non-dimensional frequency of the smart FG porous plate while, for the positive values of magnetic potential, a reverse trend is noticed. It is concluded that for MEE-FG (I) plate, the natural frequencies are influenced of the porosity which rely on the material gradation index (p). But for MEE-FG (II) plate, higher values of porosity volume fraction provide larger values of the frequency for all material graduation index. Comparing results of even and uneven porosity distributions reveals that the porosity has more considerable impact on the natural frequencies of the MEE-FG (I) than MEE-FG (II) at every magnetic potentials and electric voltages. Comparing the non-dimensional frequency of smart FG plate for different boundary conditions expresses that the greatest non-dimensional frequency is obtained for MEE-porous FG plate with CCFF boundary condition followed with other boundary conditions. In order to evaluate the effect of the porosity volume fraction on the first non-dimensional frequencies of the smart SSSS MEE-FGM-I &-II plate resting on elastic foundation, the natural frequency variation, versus the material gradation index for different volume fractions of porosity (α=0, 0.1, 0.2) at a constant values of side-to-thickness ratio (a/h=100), elastic parameter foundations (k_w=k_p=0, 10), magnetic potential (Ω=0) and electric voltage (V=0) is plotted in Figs. 3. It is found that the porosity effect on the smart FG(I)&(II) plate resting on elastic foundation is as follow: the non-dimensional frequency increases as the porosity parameter (α) increases for every value of power-law indexes. Therefore, it is clear that the porosity effect becomes outstanding for MEE-FG plate resting on elastic foundation. The impact of electric voltage and magnetic potential on the

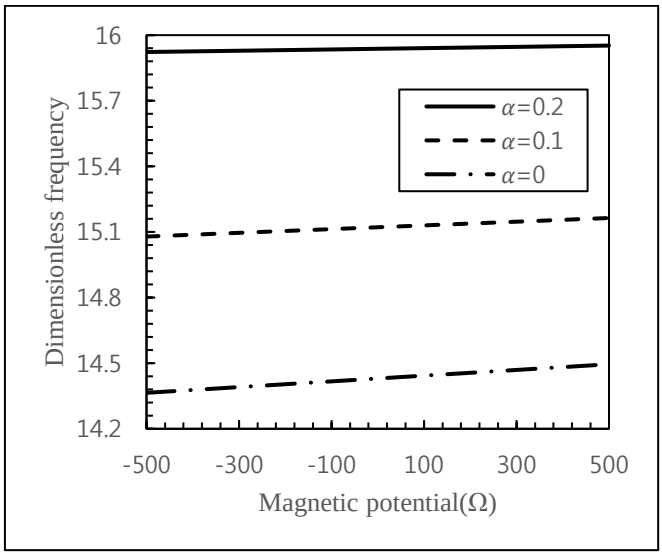

(a) even porosity

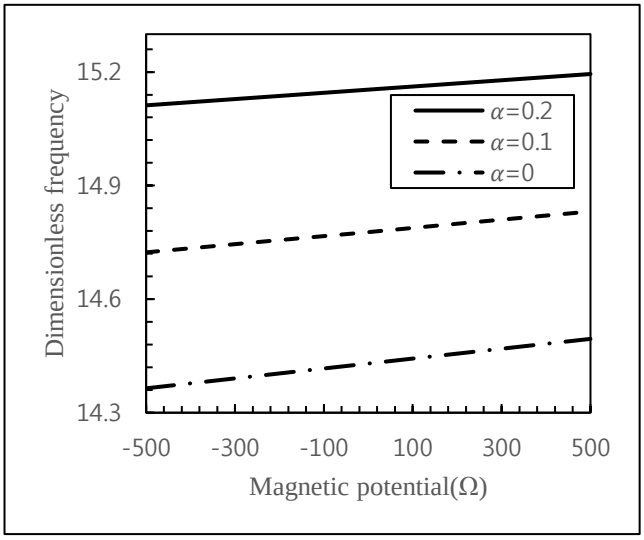

(b) uneven porosity

Fig. 5 Effect of porosity volume index on the dimensionless frequency of the SSSS MEE-FGM(I) plate on elastic foundations with respect to applied magnetics potential (a/h=100, V=0, p = 5, k_w = 10, k_p = 10)

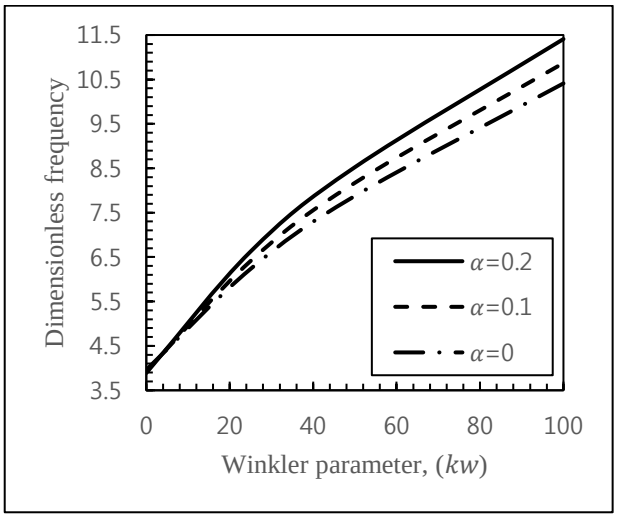

(a) SSSS, uneven porosity

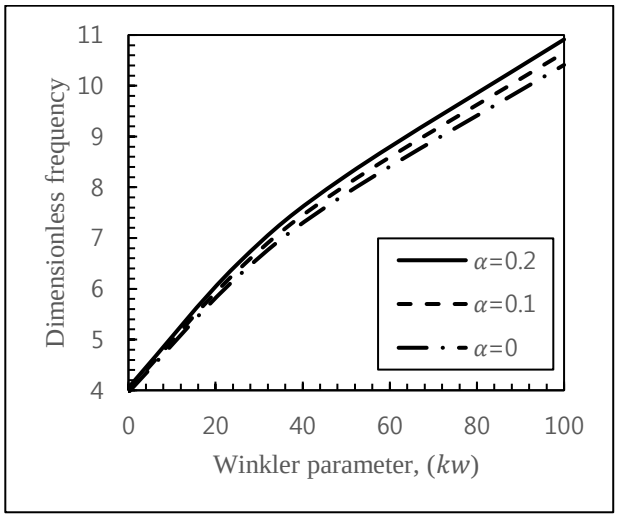

(b) SSSS, even porosity

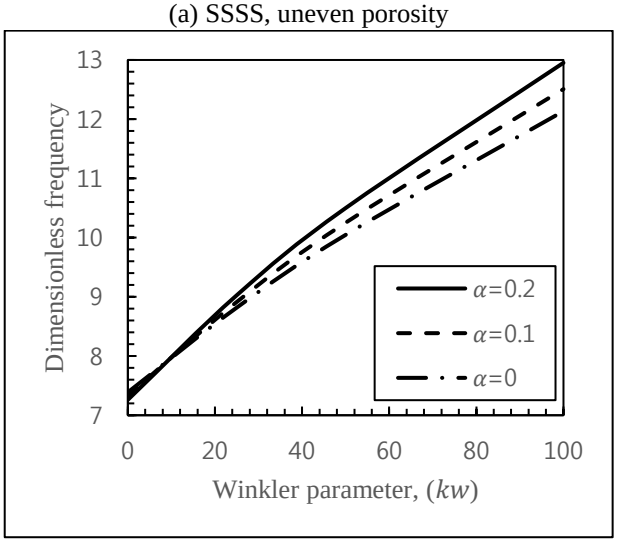

(a) CCCC, even porosity

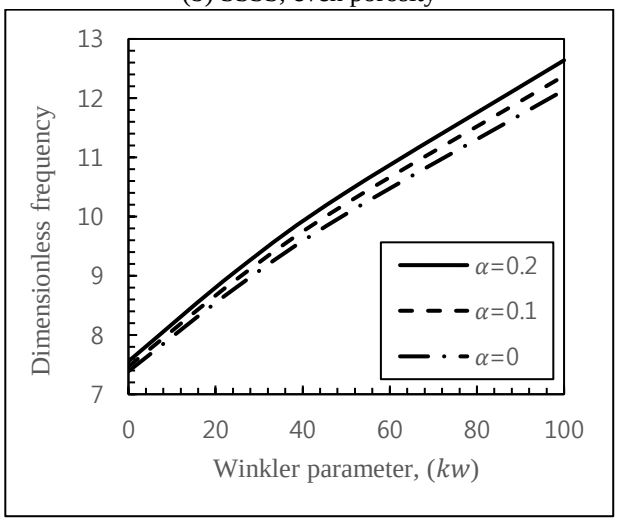

(b) CCCC, uneven porosity

Fig. 6 Influence of Winkler parameters on the dimensionless frequency of the SSSS MEE-FGM(I)&(II) plate for different porosity volume fractions and boundary conditions (a/h=100, V=200, Ω=0, p = 5, k_p = 0)

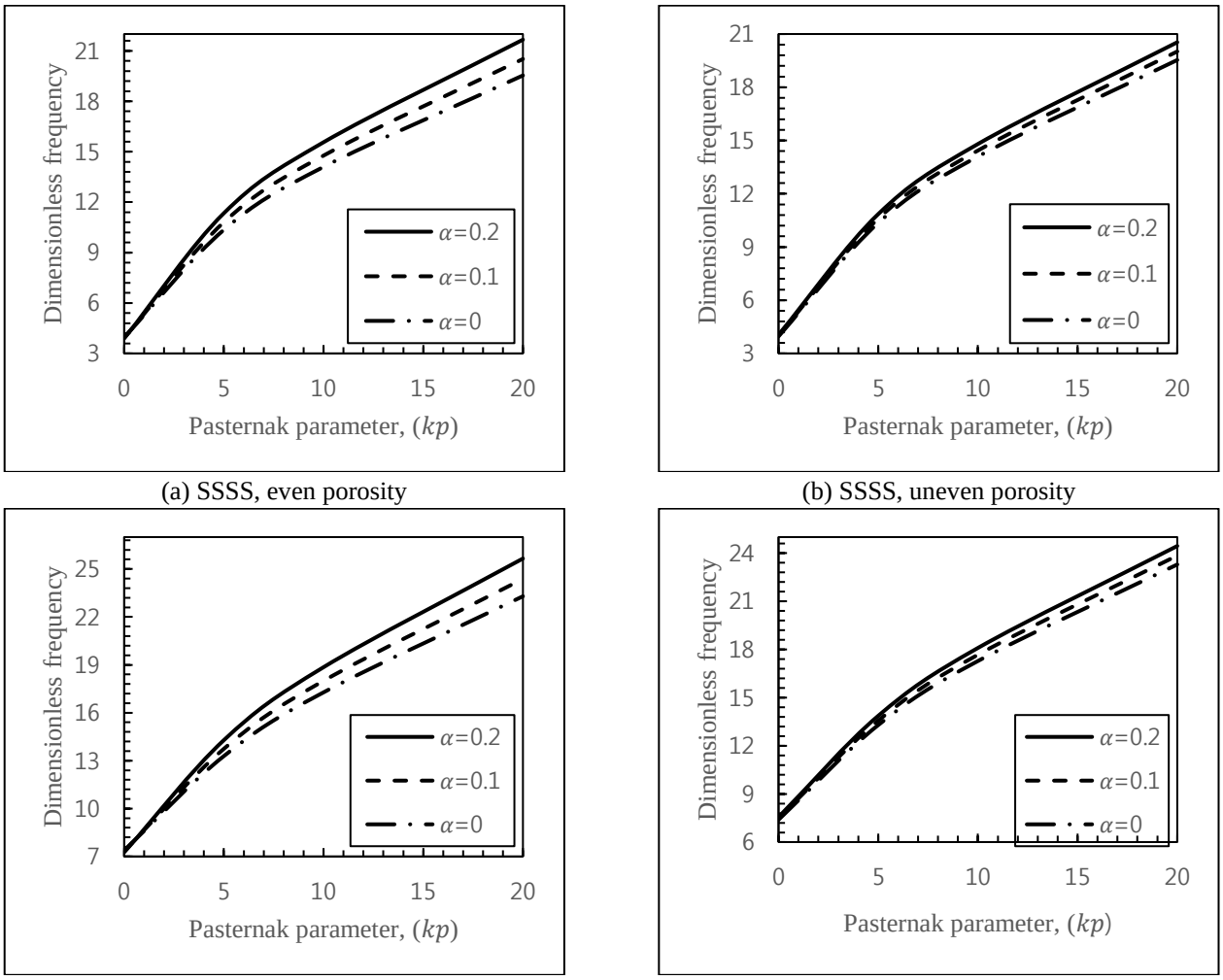

(a) SSSS, even porosity

(b) SSSS, uneven porosity

(c) CCCC, even porosity

(d) CCCC, uneven porosity

Fig. 7 Influence of Pasternak parameters on the dimensionless frequency of the SSSS MEE-FGM(I)&(II) plate for different porosity volume fractions and boundary conditions (a/h=100, V = 200, Ω=0, p = 5, k_w = 0)

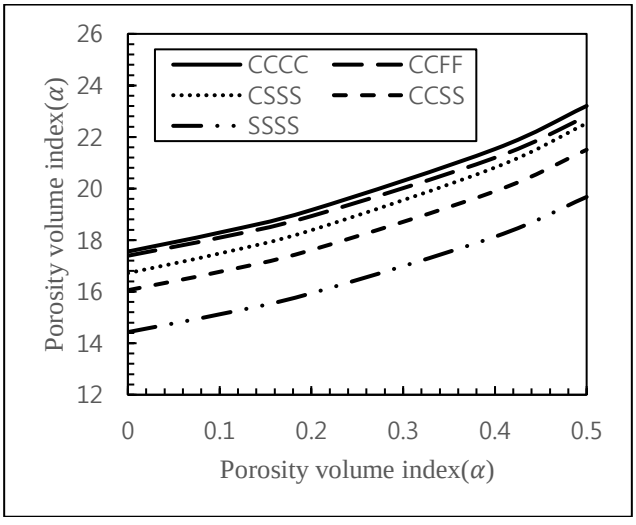

$(k_w = 10,\ k_p = 10)$

Fig. 8. Effect of porosity volume index on the dimensionless frequency of various boundary FGM(I) square plate resting on different elastic foundation parameter (a/h=100, V = 0, Ω=0, p = 5)

non-dimensional frequencies of the simply-supported smart MEE-FG plates resting on elastic foundation with even and uneven porosity distribution for different values of porosity volume fractions at (a/h=100, p = 5, k_w = 10, k_p = 10) isillustrated in Figs. 4 and 5, respectively.

It is obvious that when the intensity of external electric voltage and magnetic potential increases from negative to positive value, respectively the non-dimensional frequency of MEE porous plate reduce and increase for both porosity distributions. Also, it is observed that the impact of the

external electric voltage and magnetic potential on the non-dimensional frequency of MEE-FG(II) resting on elastic foundation is more prominent than that of the MEE-FG(I). Hence, it is very crucial to pay attention to the type of porosity distribution of MEE-FG porous plate. In addition, as can be seen with the change in the porosity volume fraction, with the presence of the elastic foundations, the non-dimensional frequency of the smart FG plate increases as the porosity parameter increases.

Figures 6 and 7 indicate the variation of the dimensionless frequency of SSSS and CCCC MEE-FG porous plate exposed to electric voltage as a function of

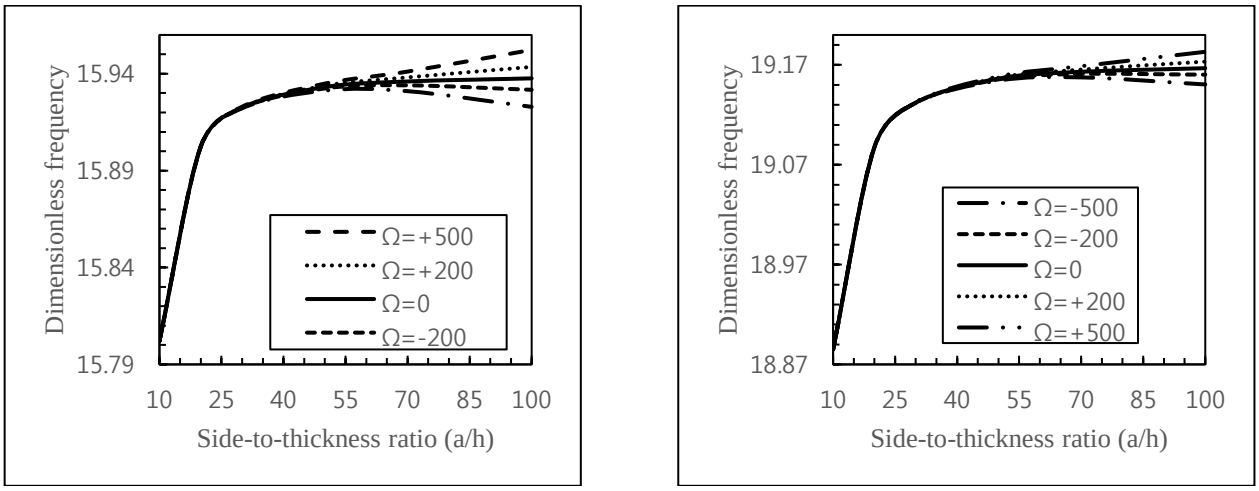

(a) SSSS, α=0.2 (b) CCCC, α=0.2

Fig. 9 Influence of side-to-thickness ratio on the dimensionless frequency of SSSS&CCCC MEE-FGM(I) square plate resting on elastic foundation for different porosity value and magnetic potentials (p = 5, k_w = 10, k_p = 10, V= 0, Ω=0)

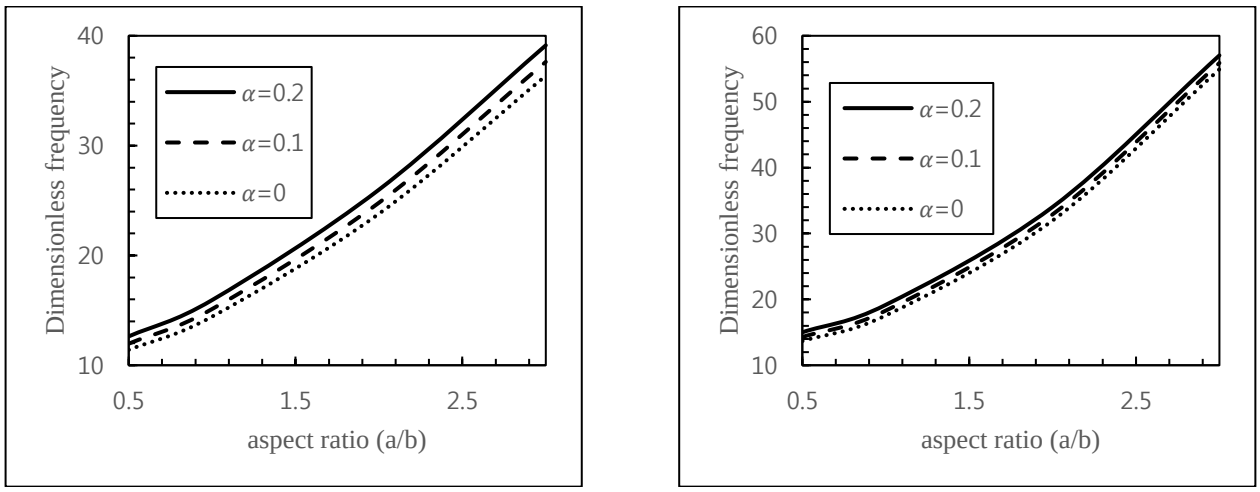

(a) SSSS (b) CCCC

Fig. 10 Effect of aspect ratio on the dimensionless frequency of SSSS&CCCC MEE-FGM(I) square plate resting on elastic foundation for different porosity volume fraction (p = 5, k_w = 10, k_p = 10, V= 0, Ω=0)

Winkler and Pasternak parameter for different porosity volume fraction (α=0, 0.1, α=0.2) and two porosity distributions (even and uneven), at (a/h=100, V=200, Ω=0,

P=5). It is known that improving the Winkler and Pasternak parameter lead to increasing of non-dimensional frequency for all of porosity volume fraction. In addition, it is found that the influence of porosity on natural frequencies of MEE-FG plate is more considerable with elastic foundation. In other words, effect of porosity is negligible at lower Winkler and Pasternak elastic parameters. Therefore, it is important to consider porosity effect in the analysis of MEE-FG plates resting on elastic foundation. In addition, it is seen that the influence of the Pasternak parameter on the non-dimensional frequency is more prominent than that of the Winkler parameter. Hence, it is very important to regard the shear layer of an elastic foundation in the analysis of MEE-FG plate with porosity.

In order to investigate the effect of porosity on the vibration of the smart MEE-FG plates with elastic foundation, variations of the non-dimensional natural frequency of SSSS MEE-FGM-I plate as a function of porosity parameter for various boundary conditions at a constant value of side-to-thickness ratio (a/h=100), elastic parameters $(k_p, k_w = 10)$, power-law index (p=5), magnetic potential (Ω=0) and electric voltage (V=0) is plotted at Fig. 8. It can be concluded that the greatest frequency of MEE-FG plate is obtained for the plate with CCCC boundary conditions followed by CCFF, CSSS, CCSS and SSSS respectively. It can be pointed that the impact of porosity volume fraction on the natural frequency of MEEE-FG (I) plate with elastic foundation is similar previous conclusions for all boundary conditions. On the other hand, improving the porosity volume fraction with existence of elastic foundation respectively provide higher natural frequencies for MEE-FG(I) plate. So, existence of elastic foundation has significant role on vibration behavior of porous MEE-FG plates.

To display the impact of side-to-thickness ratio on the

non-dimensional frequency of MEE-FG (I) plate resting on elastic foundation for various external magnetic (Ω=500, 200, 0, -200, -500), Fig.9 presents the frequency results versus side-to-thickness ratio with two boundary conditions (SSSS & CCCC) at constant value of power-law index (p=5), porosity parameter (α=0.2), Winkler & Pasternak elastic parameter (k_w = 10, k_p = 10), magnetic potential (Ω=0) and electric voltage (V=0). As can be seen, at first increment of side-thickness ratio leads to increasing of non-dimensional frequency of MEE-FG(I) for both boundary conditions and all of the magnetic potential. Then, with the increasing of a/h, it can be seen that Ω>0, Ω=0, Ω<0 provided higher, approximately constant and lower dimensional frequency, respectively. In addition, it is observable that higher values of *a/h* have more significant influence on frequency response.

Consequently, the difference between frequency results according to negative and positive values of electric and magnetic fields increases with the rise of side-to-thickness ratio. Figure 10 shows the effect of aspect ratio a/b on the natural frequency of smart MEE-FG plate resting on Winkler- Pasternak elastic foundation for different boundary conditions (SSSS&CCCC) and porosity parameters (α=0, 0.1, 0.2) at (p = 5, k_w = 10, k_p = 10, V= 0, Ω=0), respectively. It is pointed that increasing the aspect ratio is cause of increment in the non-dimensional frequencies of MEE-FG plate with even porosity for both boundary conditions.

5. Conclusions

In the present paper, vibration of porous magneto-electro-elastic functionally graded (MEE-FG) plate resting on elastic foundation with various boundary conditions is studied within the framework of a four-variable higher order shear deformation theory in which shear deformation effect is involved without the need for shear correction factors. Two types of porosity distributions, namely even and uneven are considered. Mechanical properties of the smart porous MEE-FG plate are gradually variable in the thickness direction based on modified rule of mixture. The equations of motion and boundary conditions are derived by using Hamilton principle. An analytical solution method is used to solve governing partial differential equations for various boundary conditions. It is indicated that the vibration characteristics of embedded porous MEE-FGM plate are significantly affected by various parameters such as elastic parameters, magnetic field, external electric voltage, volume fraction of porosity, material graduation, various boundary conditions and porosity distributions. Numerical results show that:

- By increasing the material graduation index value, the non-dimensional frequencies of porous MEE-FG plate are found to decrease regardless of porosity value.
- For MEE-FGM (I) plate without elastic foundation, increasing the volume fraction of porosity first yields an increase in fundamental frequency, then this trend becomes vice versa for upper values of gradient index. But with existence of elastic foundation, increasing the volume fraction of porosity increases fundamental frequency of MEE-FGM (I) plate for all values of gradient index.
- Fundamental frequency of MEE-FG(II) plate with and without elastic foundation increases with increment in porosity parameters for all values of power-law index.
- Increasing magnetic potential yields increment of non-dimensional frequency of embedded porous MEE-FGM plate. However, for the external electric voltage this behavior is opposite.
- Effect of porosity volume fraction on natural frequency depends on existence of elastic foundation, porosity distribution and power-law index.
- The non-dimensional frequency of porous MEE-FGM plate resting on elastic foundation with CCCC boundary conditions is greatest, followed by CCFF, CSSS, CCSS and SSSS respectively.
- Effect of side-to-thickness ratio (a/h) on frequencies with respect to magnetic potentials is more prominent at its higher values. As side-to-thickness ratio increases, the difference between frequency results according to negative and positive values of magnetic fields increases and this difference is more noticeable for perfect MEE-FG plate.
- With the increasing of aspect ratio, the non-dimensional frequency of porous MEE-FG plate resting on elastic foundation increase.

References

Akgoz, B. and O. Civalek (2011), "Nonlinear vibration analysis of laminated plates resting on nonlinear two-parameters elastic foundations", *Steel Compos. Struct.*, **11**(5), 403-421. https://doi.org/10.12989/scs.2011.11.5.403.

Arrigan, J., Huang, C., Staino, A., Basu, B., and Nagarajaiah, S. (2014), "A frequency tracking semi-active algorithm for control of edgewise vibrations in wind turbine blades", *Smart Struct. Syst.*, **13**(2), 177-201. https://doi.org/10.12989/sss.2014.13.2.177.

Annigeri, A.R., N. Ganesan, and S. Swarnamani (2007), "Free vibration behaviour of multiphase and layered magneto-electro-elastic beam", *J. Sound Vib.*, **299**(1), 44-63. https://doi.org/10.1016/j.jsv.2006.06.044.

Atmane, H.A., A. Tounsi, and F. Bernard (2015), "Effect of thickness stretching and porosity on mechanical response of a functionally graded beams resting on elastic foundations", *J. Mech. Mater. Design*, 1-14. https://doi.org/10.1007/s10999-015-9318-x.

Beldjelili, Y., Tounsi, A., and Mahmoud, S.R. (2016), "Hygro-thermo-mechanical bending of S-FGM plates resting on variable elastic foundations using a four-variable trigonometric plate theory", *Smart Struct. Syst.*., **18**(4), 755-786. https://doi.org/10.12989/sss.2016.18.4.755.

Boutahar, L. and R. Benamar (2016), "A homogenization procedure for geometrically non-linear free vibration analysis of functionally graded annular plates with porosities, resting on elastic foundations", *Ain Shams Eng. J.*, **7**(1), 313-333. https://doi.org/10.1016/j.asej.2015.11.016.

Bouafia, K., Kaci, A., Houari, M. S. A., Benzair, A., and Tounsi, A. (2017), "A nonlocal quasi-3D theory for bending and free flexural vibration behaviors of functionally graded nanobeams", *Smart Struct. Syst.*., **19**(2), 115-126. https://doi.org/10.12989/sss.2017.19.2.115.

Bjurström, H., Ryden, N., and Birgisson, B. (2016), "Non-contact surface wave testing of pavements: comparing a rolling microphone array with accelerometer measurements", *Smart*

Struct. Syst., **17**(1), 1-15. https://doi.org/10.12989/sss.2016.17.1.001.

Benveniste, Y. (1995), "Magnetoelectric effect in fibrous composites with piezoelectric and piezomagnetic phases", *Physical Review B*, **51**(22). https://doi.org/10.1103/PhysRevB.51.16424.

Chikh, A., Tounsi, A., Hebali, H. and Ma hmoud, S.R. (2017), "Thermal buckling analysis of cross-ply laminated plates using a simplified HSDT", *Smart Struct. Syst.*, **19**(3), 289-297. https://doi.org/10.12989/sss.2017.19.3.289.

Chen, W., K.Y. Lee, and H. Ding (2005), "On free vibration of non-homogeneous transversely isotropic magneto-electro-elastic plates", *J. Sound Vib.*, **279**(1), 237-251. https://doi.org/10.1016/j.jsv.2003.10.033.

Civalek, Ö. (2007), "Nonlinear analysis of thin rectangular plates on Winkler–Pasternak elastic foundations by DSC–HDQ methods", *Appl. Math. Modell.*, **31**(3), 606-624. https://doi.org/10.1016/j.apm.2005.11.023.

Civalek, Ö. (2006), "Harmonic differential quadrature-finite differences coupled approaches for geometrically nonlinear static and dynamic analysis of rectangular plates on elastic foundation", *J. Sound Vib.*, **294**(4), 966-980. https://doi.org/10.1016/j.jsv.2005.12.041.

Daga, A., N. Ganesan, and K. Shankar (2009), "Transient dynamic response of cantilever magneto-electro-elastic beam using finite elements", *J. Comput. Method. Eng. Sci. Mech.*, **10**(3), 173-185. https://doi.org/10.1080/15502280902797207.

Ebrahimi, F. and M. Mokhtari (2014), "Transverse vibration analysis of rotating porous beam with functionally graded microstructure using the differential transform method", *J. Brazil. Soc. Mech. Sci. Eng.*, 1-10. https://doi.org/10.1007/s40430-014-0255-7.

Ebrahimi, F. and M. Zia (2015), "Large amplitude nonlinear vibration analysis of functionally graded Timoshenko beams with porosities", *Acta Astronautica*, **116**, 117-125. https://doi.org/10.1016/j.actaastro.2015.06.014.

Ebrahimi, F., F. Ghasemi, and E. Salari (2016), "Investigating thermal effects on vibration behavior of temperature-dependent compositionally graded Euler beams with porosities", *Meccanica*, **51**(1), 223-249. https://doi.org/10.1007/s11012-015-0208-y.

Glaser, S.D., Shoureshi, R.A. and Pescovitz, D. (2005), "Frontiers in sensors and sensing systems", *Smart Struct. Syst.*, **1**(1), 103-120.

Huang, D., H. Ding, and W. Chen (2007), "Analytical solution for functionally graded magneto-electro-elastic plane beams", *J. Eng. Sci.*, **45**(2), 467-485. https://doi.org/10.1016/j.ijengsci.2007.03.005.

Huang, Z., C. Lü, and W. Chen (2008), "Benchmark solutions for functionally graded thick plates resting on Winkler–Pasternak elastic foundations", *Compos. Struct.*, **85**(2), 95-104. https://doi.org/10.1016/j.compstruct.2007.10.010.

Hashemi, S.H., H.R.D. Taher and M. Omidi (2008), "3-D free vibration analysis of annular plates on Pasternak elastic foundation via p-Ritz method", *J. Sound Vib.*, **311**(3), 1114-1140. https://doi.org/10.1016/j.jsv.2007.10.020.

Karami B, Shahsavari D and Li, L, (2018), "Temperature-dependent flexural wave propagation in nanoplate-type porous heterogenous material subjected to in-plane magnetic field", *J. Thermal Stress,* **41**(4), 483-499. https://doi.org/10.1080/01495739.2017.1393781.

Kim, R.E., Moreu, F., and Spencer, B.F. (2015), "System identification of an in-service railroad bridge using wireless smart sensors", *Smart Struct. Syst.*, **15**(3), 683-698. https://doi.org/10.12989/sss.2015.15.3.683.

Ke, L.-L. and Y.-S. Wang (2014), "Free vibration of size-dependent magneto-electro-elastic nanobeams based on the nonlocal theory", *Physica E Low Diemnsional Syst. Nanostruct.*, **63**, 52-61. https://doi.org/10.1016/j.physe.2014.05.002.

Kattimani, S. and M. Ray (2015), "Control of geometrically nonlinear vibrations of functionally graded magneto-electro-elastic plates", *J. Mech. Sci.*, **99**, 154-167. https://doi.org/10.1016/j.ijmecsci.2015.05.012.

Kumaravel, A., N. Ganesan, and R. Sethuraman (2007), "Buckling and vibration analysis of layered and multiphase magneto-electro-elastic beam under thermal environment", *Multidiscipline Model. Mater. Struct.*, **3**(4), 461-476. https://doi.org/10.1163/157361107782106401.

Liu, M.F. and T.P. Chang (2010), "Closed form expression for the vibration problem of a transversely isotropic magneto-electro-elastic plate", *J. Appl. Mech.*, **77**(2). https://doi.org/10.1115/1.3176996.

Malekzadeh, P. (2009), "Three-dimensional free vibration analysis of thick functionally graded plates on elastic foundations", *Compos. Struct.*, **89**(3), 367-373. https://doi.org/10.1016/j.compstruct.2008.08.007.

Mechab, I., Mechab, B., Benaissa, S., Serier, B. and Bouiadjra, B. B. (2016), "Free vibration analysis of FGM nanoplate with porosities resting on Winkler Pasternak elastic foundations based on two-variable refined plate theories", *J. Brazil. Soc. Mech. Sci. Eng.* 1-19. https://doi.org/10.1007/s40430-015-0482-6.

Mantari, J., E. Bonilla, and C.G. Soares (2014), "A new tangential-exponential higher order shear deformation theory for advanced composite plates", *Compos. Part B*, **60**, 319-328. https://doi.org/10.1016/j.compositesb.2013.12.001.

Ochs, S., Li, S., Adams, C., and Melz, T. (2017), "Efficient Experimental Validation of Stochastic Sensitivity Analyses of Smart Systems", *Smart Struct. Mater.*, 97-113. https://doi.org/10.1007/978-3-319-44507-6_5.

Peng, X., M. Yan, and W. Shi, (2007), "A new approach for the preparation of functionally graded materials via slip casting in a gradient magnetic field", *Scripta materialia*, **56**(10), 907-909. https://doi.org/10.1016/j.scriptamat.2006.12.020.

Providakis, C. P., Triantafillou, T. C., Karabalis, D., Papanicolaou, A., Stefanaki, K., Tsantilis, A. and Tzoura, E. (2014). "Simulation of PZT monitoring of reinforced concrete beams retrofitted with CFRP", *Smart Struct. Syst.*, **14**(5), 811-830. https://doi.org/10.12989/sss.2014.14.5.811.

Pan, E. and Han, F. (2005), "Exact solution for functionally graded and layered magneto-electro-elastic plates", *J. Eng. Sci.*, **43**(3), 321-339. https://doi.org/10.1016/j.ijengsci.2004.09.006.

Pradhan, S. and T. Murmu (2009), "Thermo-mechanical vibration of FGM sandwich beam under variable elastic foundations using differential quadrature method", *J. Sound Vib.*, **321**(1), 342-362. https://doi.org/10.1016/j.jsv.2008.09.018.

Razavi, S. and A. Shooshtari (2015), "Nonlinear free vibration of magneto-electro-elastic rectangular plates", *Compos. Struct.*, 377-384. https://doi.org/10.1016/j.compstruct.2014.08.034.

Rezaei, A. and A. Saidi (2016), "Application of Carrera Unified Formulation to study the effect of porosity on natural frequencies of thick porous–cellular plates", *Compos. Part B*, **91**, 361-370. https://doi.org/10.1016/j.compositesb.2015.12.050.

Shahsavari, D., Shahsavari, M., Li, L. and Karami, B. (2018), "A novel quasi-3D hyperbolic theory for free vibration of FG plates with porosities resting on Winkler/Pasternak/Kerr foundation", *Aerosp. Sci. Technol.,* **72**, 134-149. https://doi.org/10.1016/j.ast.2017.11.004.

Sobhy, M. (2013), "Buckling and free vibration of exponentially graded sandwich plates resting on elastic foundations under various boundary conditions", *Compos. Struct.*, **99**, 76-87. https://doi.org/10.1016/j.compstruct.2012.11.018.

Sladek, J., Sladek, V., Krahulec, S., Chen, C.S. and Young, D.L. (2015), "Analyses of Circular Magnetoelectroelastic Plates with Functionally Graded Material Properties", *Mech. Adv. Mater. Struct.*,

22(6), 479-489. https://doi.org/10.1080/15376494.2013.807448.

Tang, H., Li, L. and Hu, Y. (2018), "Buckling analysis of two-directionally porous beam", *Aerosp. Sci. Technol.,* **78**, 471-479. https://doi.org/10.1016/j.ast.2018.04.045.

Tiwari, R., Kim, K.J., and Kim, S.M. (2008), "Ionic polymer-metal composite as energy harvesters", *Smart Struct. Syst.*, **4**(5), 549-563. https://doi.org/10.12989/sss.2008.4.5.549.

Thai, H. T., and Choi, D. H. (2012), "A refined shear deformation theory for free vibration of functionally graded plates on elastic foundation", *Compos. Part B*, **43**(5), 2335-2347. https://doi.org/10.1016/j.compositesb.2011.11.062.

Vinyas, M. and Kattimani, S.C. (2017a), "Static studies of stepped functionally graded magneto-electro-elastic beam subjected to different thermal loads", *Compos. Struct.,* **163**, 216-237. https://doi.org/10.1016/j.compstruct.2016.12.040.

*Vi*nyas, M. and Kattimani, S.C. (2017b), "A Finite element based assessment of static behavior of multiphase magneto-electro-elastic beams under different thermal loading", *Struct. Eng. Mech*., **62**(5), 519-535. https://doi.org/10.12989/sem.2017.62.5.519.

Vinyas, M. and Kattimani, S.C. (2017c), "Static behavior of thermally loaded multilayered Magneto-Electro-Elastic beam", *Struct. Eng. Mech*., **63**(4), 481-495. https://doi.org/10.12989/sem.2017.63.4.481.

Vinyas, M. and Kattimani, S.C. (2017d), "Multiphysics response of magneto-electro-elastic beams in thermo-mechanical environment", *Coupled Syst. Mech.,* **6**(3), 351-368. https://doi.org/10.12989/csm.2017.6.3.351.

Vinyas, M. and Kattimani, S.C. (2017e), "A 3D finite element static and free vibration analysis of magneto-electro-elastic beam", *Coupled Syst. Mech*, **6**(4), 465-485. https://doi.org/10.12989/csm.2017.6.4.465.

Vinyas, M. and Kattimani, S.C. (2017f), "Static analysis of stepped functionally graded magneto-electro-elastic plates in thermal environment: A finite element study", *Compos. Struct.* **178**, 63-85. https://doi.org/10.1016/j.compstruct.2017.06.068.

*Vi*nyas, M. and Kattimani, S.C. (2017g), "Hygrothermal analysis of magneto-electro-elastic plate using 3D finite element analysis", *Compos. Struct.,* **180**, 617-637. https://doi.org/10.1016/j.compstruct.2017.08.015.

*Vi*nyas, M. and Kattimani, S.C. (2018), "Finite element evaluation of free vibration characteristics of magneto-electro-elastic rectangular plates in hygrothermal environment using higher-order shear deformation theory", *Compos. Struct.*, **202**, 1339-1352. https://doi.org/10.1016/j.compstruct.2018.06.069.

Wattanasakulpong, N. and Ungbhakorn, V. (2014), "Linear and nonlinear vibration analysis of elastically restrained ends FGM beams with porosities", *Aerosp. Sci. Technol.*, **32**(1), 111-120. https://doi.org/10.1016/j.ast.2013.12.002.

Wu, C.P. and Y.H. Tsai (2007), "Static behavior of functionally graded magneto-electro-elastic shells under electric displacement and magnetic flux", *J. Eng. Sci.*, **45**(9), 744-769. https://doi.org/10.1016/j.ijengsci.2007.05.002.

Wattanasakulpong, N. and A. Chaikittiratana (2015), "Flexural vibration of imperfect functionally graded beams based on Timoshenko beam theory: Chebyshev collocation method", *Meccanica*, 1-12. https://doi.org/10.1007/s11012-014-0094-8.

Wattanasakulpong, N., Prusty, B.G., Kelly, D.W. and Hoffman, M. (2012), "Free vibration analysis of layered functionally graded beams with experimental validation", *Mater. Design*, **36**, 182-190. https://doi.org/10.1016/j.matdes.2011.10.049.

Xiang, Z., Chan, T. H., Thambiratnam, D. P. and Nguyen, T. (2016), "Synergic identification of prestress force and moving load on prestressed concrete beam based on virtual distortion method", *Smart Struct. Syst.*, **17**(6), 917-933. https://doi.org/10.12989/sss.2016.17.6.917.

Xin, L. and Z. Hu (2015), "Free vibration of layered magneto-electro-elastic beams by SS-DSC approach", *Compos. Struct.*, **125**, 96-103. https://doi.org/10.1016/j.compstruct.2015.01.048.

Ying, Z. G., Ni, Y. Q. and Duan, Y. F. (2017), "Stochastic vibration suppression analysis of an optimal bounded controlled sandwich beam with MR visco-elastomer core", *Smart Struct. Syst.*, **19**(1), 21-31. https://doi.org/10.12989/sss.2017.19.1.021.

Ying, J., C. Lü, and W. Chen (2008), "Two-dimensional elasticity solutions for functionally graded beams resting on elastic foundations", *Compos. Struct.*, **84**(3), 209-219. https://doi.org/10.1016/j.compstruct.2007.07.004.

Yun, G.J., Ogorzalek, K.A., Dyke, S.J., and Song, W. (2009), "A two-stage damage detection approach based on subset selection and genetic algorithms", *Smart Struct. Syst.*, **5**(1), 1-21. https://doi.org/10.12989/sss.2009.5.1.001.

Yi, T. H., Li, H. N. and Gu, M. (2013), "Wavelet based multi-step filtering method for bridge health monitoring using GPS and accelerometer", *Smart Struct. Syst.*, **11**(4), 331-348. https://doi.org/10.12989/sss.2013.11.4.331.

Zhu, J., Lai, Z., Yin, Z., Jeon, J. and Lee, S. (2001), "Fabrication of ZrO 2–NiCr functionally graded material by powder metallurgy", *Mater. Chem. Phys.*, 2001. **68**(1), 130-135. https://doi.org/10.1016/S0254-0584(00)00355-2.

Zhou, D., Lo, S. H., Au, F. T. K. and Cheung, Y. K. (2006), "Three-dimensional free vibration of thick circular plates on Pasternak foundation", *J. Sound Vib.*, **292**(3), 726-741. https://doi.org/10.1016/j.jsv.2005.08.028.

Zhou, Y. G., Chen, Y. M., and Ding, H. J. (2005), "Analytical solutions to piezoelectric bimorphs based on improved FSDT beam model", *Smart Struct. Syst.*, **1**(3), 309-324. https://doi.org/10.12989/sss.2005.1.3.309.

CC